

An advanced meshless approach for the high-dimensional multi-term time-space-fractional partial differential equation on general domain

Xiaogang Zhu^{a,*}, Jungang Wang^b, Zhanbin Yuan^b, Yufeng Nie^b

^a*School of Science, Shaoyang University, Shaoyang, Hunan 422000, P.R. China*

^b*Department of Applied Mathematics, Northwestern Polytechnical University, Xi'an, Shaanxi 710129, P.R. China*

Abstract

The mathematical models built based on time- and space-fractional derivatives adequately describe the phenomena incorporating temporal-spatial heterogeneity, but how to obtain their solutions on general domains remains a difficult issue. In this article, an advanced differential quadrature (DQ) approach is proposed for the high-dimensional multi-term time-space-fractional partial differential equations (TSFPDEs) on general domains. Firstly, a new class of DQ formulas is derived to evaluate the fractional derivatives in space, which utilize radial basis functions (RBFs) as trial functions. With these DQ formulas, the original problems are then converted to a group of multi-term fractional ordinary differential equations (ODEs) and they are further discretized by a family of high-order difference schemes based on Lubich's difference operators. The proposed DQ method provides a flexible and high accurate alternative to solve the high-dimensional multi-term TSFPDEs on general domains and its actual performance is illustrated by the benchmark tests on square, triangular, elliptical, triangular pyramid and sphere domains or by contrast to the other methods in open literature. The numerical results finally confirm its capability and advantages.

Keywords: radial basis functions, differential quadrature, multi-term time-space fractional partial differential equation.

1. Introduction

During the last ten years, fractional calculus came into the focus of interest in academic circles as an important branch of mathematics. Due to its non-locality and self-similarity, it has been proven to be very adequate to characterize the dynamics phenomena associated with temporal memory or long-range space interaction like the anomalous transport in heterogeneous aquifer [1]. The application of fractional calculus has been very extensive in modelling processes in applied sciences, including biology, chemistry, physics, economics, and many other disciplines.

The fractional partial differential equations (PDEs) are the results of mathematical modelling based on the fractional calculus, which provides a new powerful tool to study some complex systems in mathematical physics or even the whole scientific research. Nevertheless, there raises a challenge to solve these type of equations and few of fractional PDEs can be solved by analytic techniques. As a result, numerical methods are clearly priority for development. Up to present, the numerical algorithms for the time-fractional PDEs are on the way to maturity after recent years' development [20, 21, 23, 26, 33, 40, 45, 48], while these for the high-dimensional space-fractional PDEs have to be further developed and improved, especially for the ones defined on general domains. Regardless of the difficulties in constructing numerical algorithms for the space-fractional PDEs, many numerical methods have been invented to solve them, covering finite difference (FD) methods [7, 22, 32, 42], spectral methods [5, 46], finite element (FE) methods [13, 15, 47, 49], and finite volume methods [18, 41]. Liu et al. considered a space-fractional FitzHugh-Nagumo monodomain model by an implicit semi-alternative direction FD scheme on approximate irregular domains [29]. Qiu et al. developed a nodal discontinuous Galerkin method for the two-dimensional space-fractional diffusion

*Corresponding author

Email address: zhuxg590@yeah.net (Xiaogang Zhu)

equations and solved a L-shaped domain problem [38]. Yang et al. studied a FE method for the two-dimensional non-linear space-fractional diffusion equations on convex domains [44]. Bhrawy and Zaky developed a Jacobi spectral tau method for the multi-term TSFPDEs [6]. In [12], an efficient numerical algorithm based on FD and FE methods was addressed for the two-dimensional multi-term time-space-fractional Bloch-Torrey equations. Qin et al. gave a fully discrete FE scheme for the multi-term time and space fractional Bloch-Torrey equation based on bilinear rectangular finite elements [37]. Fan et al. proposed a fully discrete FE scheme with unstructured meshes for the two-dimensional multi-term time-space fractional diffusion-wave equations on irregular domains [16].

Although the study of numerical methods for the fractional PDEs is an active area of research, few works have been reported for the high-dimensional multi-term TSFPDEs on general domains. Actually, this topic is full of challenges because of the non-locality and weakly singular integral kernel of fractional derivatives, which is the biggest difficulty in the design of their numerical algorithms. The currently available algorithms are either limited to regular domain problems or suffer from the shortcoming of high complexity and heavy computing burden. This situation motivates us to seek another efficient numerical methods to solve these equations. Meshless methods eliminate the tedious mesh generation and reconstruction or only use easily generable meshes in a flexible manner, and thereby reduce the computational cost in practise. They serve as promising alternatives in dealing with the structure destruction, high-dimensional crack propagation, and large deformation problems. In the past two decades, meshless methods have achieved significant advances and many meshless methods have been developed, such as diffuse element method [34], reproducing kernel particle (RKP) method [19], hp-cloud method, element-free Galerkin method [4], meshless local Petrov-Galerkin method [2], boundary element-free method, Kansa's methods [17, 24], point interpolation (PI) method [30], and so forth. Meshless methods offer more advantages over the mesh-dependent methods in treating the space-fractional PDEs but seldom works have been reported in this field, let alone the multi-term TSFPDEs. Liu et al. addressed a meshless technique based on PI method for the space-fractional diffusion equation [31]. Cheng et al. proposed an improved moving least-squares collocation scheme for the two-dimensional two-sided space-fractional wave equation [11]. Pang et al. extended the classical polynomial DQ method to solve the steady-state space-fractional advection-diffusion equations [36], where the Lagrange interpolating basis functions are used as the trial functions to determine weighted coefficients. In [27], a RKP method was developed for the two-dimensional time-space-fractional diffusion equations on irregular domains in conjunction with a matrix transfer technique.

Among various meshless methods, of particular note is DQ method [3], which has originated from the concept of quadrature approximation. Unlike the other meshless methods, DQ method employs the weighted sum of functional values at sampling nodes along ordinate directions to discretize derivatives and achieves high accuracy with a few nodes. The determination of weighted coefficients is an crucial step and the basis functions like splines, orthogonal polynomials [39], Lagrange interpolating polynomials [14], RBFs [43], and Hermite polynomials [10], have been used by many authors as trial functions. This kind of method enjoys the advantages as simpleness in its principle, easy programming, and high adaptability to high-dimensional problems. In the light of these points, we will showcase an efficient RBFs-based DQ method for the multi-term TSFPDEs on general domains:

(i) two-dimensional multi-term TSFPDE:

$$\begin{cases} P_{\theta_1, \theta_2, \dots, \theta_s}({}_0^C \mathcal{D}_t)u(x, y, t) - \varepsilon_\alpha^+(x, y) \frac{\partial^\alpha u(x, y, t)}{\partial x_+^\alpha} - \varepsilon_\alpha^-(x, y) \frac{\partial^\alpha u(x, y, t)}{\partial x_-^\alpha} \\ - \varepsilon_\beta^+(x, y) \frac{\partial^\beta u(x, y, t)}{\partial y_+^\beta} - \varepsilon_\beta^-(x, y) \frac{\partial^\beta u(x, y, t)}{\partial y_-^\beta} = f(x, y, t), & (x, y, t) \in \Omega \times (0, T], \\ u(x, y, 0) = u_0(x, y), & (x, y) \in \Omega, \\ u(x, y, t) = g(x, y, t), & (x, y, t) \in \partial\Omega \times (0, T], \end{cases} \quad (1.1)$$

where $0 < \theta_1, \theta_2, \dots, \theta_s \leq 1$, $s \in \mathbb{Z}^+$, $1 < \alpha, \beta \leq 2$, $\Omega \subset \mathbb{R}^2$ with $\partial\Omega$ being its boundary, $\varepsilon_\zeta^\pm(x, y)$ are the diffusion coefficients with $\zeta = \alpha, \beta$.

(ii) three-dimensional multi-term TSFPDE:

$$\begin{cases} P_{\theta_1, \theta_2, \dots, \theta_s}({}_0^C \mathcal{D}_t)u(x, y, z, t) - \varepsilon_\alpha^+(x, y, z) \frac{\partial^\alpha u(x, y, z, t)}{\partial x_+^\alpha} - \varepsilon_\alpha^-(x, y, z) \frac{\partial^\alpha u(x, y, z, t)}{\partial x_-^\alpha} - \varepsilon_\beta^+(x, y, z) \frac{\partial^\beta u(x, y, z, t)}{\partial y_+^\beta} \\ - \varepsilon_\beta^-(x, y, z) \frac{\partial^\beta u(x, y, z, t)}{\partial y_-^\beta} - \varepsilon_\gamma^+(x, y, z) \frac{\partial^\gamma u(x, y, z, t)}{\partial z_+^\gamma} - \varepsilon_\gamma^-(x, y, z) \frac{\partial^\gamma u(x, y, z, t)}{\partial z_-^\gamma} = f(x, y, z, t), \quad (x, y, z, t) \in \Omega \times (0, T], \\ u(x, y, z, 0) = u_0(x, y, z), \quad (x, y, z) \in \Omega, \\ u(x, y, z, t) = g(x, y, z, t), \quad (x, y, z, t) \in \partial\Omega \times (0, T], \end{cases} \quad (1.2)$$

where $0 < \theta_1, \theta_2, \dots, \theta_s \leq 1$, $s \in \mathbb{Z}^+$, $1 < \alpha, \beta, \gamma \leq 2$, $\Omega \subset \mathbb{R}^3$ with $\partial\Omega$ being its boundary, $\varepsilon_\varsigma^\pm(x, y, z)$ are the diffusion coefficients with $\varsigma = \alpha, \beta, \gamma$.

The fractional derivatives in Eqs. (1.1)-(1.2) are defined in Caputo sense. More precisely, the ones tagged with "+" are the left-side fractional derivatives, while those tagged with "-" are the right-side fractional derivatives. For example, assuming $C_1 : x = x_L(y, z)$, $C_2 : x = x_R(y, z)$ the left and right boundaries of $\Omega \subset \mathbb{R}^3$, in which,

$$\begin{aligned} x_L(y, z) &= \min\{x : (x, \eta, \zeta), \eta = y, \zeta = z\}, \\ x_R(y, z) &= \max\{x : (x, \eta, \zeta), \eta = y, \zeta = z\}, \end{aligned}$$

then $\frac{\partial^\alpha u(x, y, z, t)}{\partial x_+^\alpha}$, $\frac{\partial^\alpha u(x, y, z, t)}{\partial x_-^\alpha}$ are defined as follows:

$$\begin{aligned} \frac{\partial^\alpha u(x, y, z, t)}{\partial x_+^\alpha} &= \frac{1}{\Gamma(2-\alpha)} \int_{x_L(y, z)}^x \frac{\partial^2 u(\xi, y, z, t)}{\partial \xi^2} \frac{d\xi}{(x-\xi)^{\alpha-1}}, \\ \frac{\partial^\alpha u(x, y, z, t)}{\partial x_-^\alpha} &= \frac{1}{\Gamma(2-\alpha)} \int_x^{x_R(y, z)} \frac{\partial^2 u(\xi, y, z, t)}{\partial \xi^2} \frac{d\xi}{(\xi-x)^{\alpha-1}}, \end{aligned}$$

with the Gamma function $\Gamma(\cdot)$.

The fractional derivatives in the other coordinate directions can be defined in the same fashion. $P_{\theta_1, \theta_2, \dots, \theta_s}({}_0^C \mathcal{D}_t)$ denotes the multi-term fractional derivative operator:

$$P_{\theta_1, \theta_2, \dots, \theta_s}({}_0^C \mathcal{D}_t)u(x, y, z, t) = \sum_{r=1}^s a_{r0} {}^C D_t^{\theta_r} u(x, y, z, t) \quad (1.3)$$

$$= a_{10} {}^C D_t^{\theta_1} u(x, y, z, t) + a_{20} {}^C D_t^{\theta_2} u(x, y, z, t) + \dots + a_{s0} {}^C D_t^{\theta_s} u(x, y, z, t), \quad (1.4)$$

where

$${}_0^C D_t^{\theta_r} u(x, y, z, t) = \frac{1}{\Gamma(1-\theta_r)} \int_0^t \frac{\partial u(x, y, z, \xi)}{\partial \xi} \frac{d\xi}{(t-\xi)^{\theta_r}}.$$

The layout of this article is as follows. In Section 2, some preliminaries on the fractional calculus and RBFs are introduced. In Section 3, the DQ formulas for fractional derivatives are proposed based on different kinds of RBFs. In Section 4, with these RBFs-based DQ formulas, we construct a fully discrete DQ scheme for the multi-term TSFPDEs on general domains and its algorithm is further investigated. In Section 5, some illustrative examples are carried out to confirm its validity and convergence. In the last section, a brief summary is drawn.

2. Preliminaries

We recall some basic preliminaries on the fractional calculus and RBFs required for further discussions.

2.1. Fractional calculus

Definition 2.1. The left and right Riemann-Liouville fractional integrals of order α are defined by

$$\begin{aligned} {}_a J_x^\alpha u(x) &= \frac{1}{\Gamma(\alpha)} \int_a^x \frac{u(\xi) d\xi}{(x-\xi)^{1-\alpha}}, \quad x > a, \\ {}_x J_b^\alpha u(x) &= \frac{1}{\Gamma(\alpha)} \int_x^b \frac{u(\xi) d\xi}{(\xi-x)^{1-\alpha}}, \quad x < b, \end{aligned}$$

and if $\alpha = 0$, ${}_a J_x^\alpha u(x) = u(x)$ and ${}_x J_b^\alpha u(x) = u(x)$.

Definition 2.2. The left and right Riemann-Liouville fractional derivatives of order α are defined by

$$\begin{aligned} {}_a^{RL} D_x^\alpha u(x) &= \left(\frac{d}{dx} \right)^m {}_a J_x^{m-\alpha} u(x) = \frac{1}{\Gamma(m-\alpha)} \frac{d^m}{dx^m} \int_a^x \frac{u(\xi) d\xi}{(x-\xi)^{\alpha-m+1}}, \quad x > a, \\ {}_x^{RL} D_b^\alpha u(x) &= (-1)^m \left(\frac{d}{dx} \right)^m {}_x J_b^{m-\alpha} u(x) = \frac{(-1)^m}{\Gamma(m-\alpha)} \frac{d^m}{dx^m} \int_x^b \frac{u(\xi) d\xi}{(\xi-x)^{\alpha-m+1}}, \quad x < b, \end{aligned}$$

where $m-1 < \alpha < m$, $m \in \mathbb{Z}^+$, and if $\alpha = m$, ${}_a^{RL} D_x^\alpha u(x) = u^{(m)}(x)$ and ${}_x^{RL} D_b^\alpha u(x) = (-1)^m u^{(m)}(x)$.

Definition 2.3. The left and right Caputo fractional derivatives of order α are defined by

$$\begin{aligned} {}_a^C D_x^\alpha u(x) &= {}_a J_x^{m-\alpha} u^{(m)}(x) = \frac{1}{\Gamma(m-\alpha)} \int_a^x \frac{u^{(m)}(\xi) d\xi}{(x-\xi)^{\alpha-m+1}}, \quad x > a, \\ {}_x^C D_b^\alpha u(x) &= (-1)^m {}_x J_b^{m-\alpha} u^{(m)}(x) = \frac{(-1)^m}{\Gamma(m-\alpha)} \int_x^b \frac{u^{(m)}(\xi) d\xi}{(\xi-x)^{\alpha-m+1}}, \quad x < b, \end{aligned}$$

where $m-1 < \alpha < m$, $m \in \mathbb{Z}^+$, and if $\alpha = m$, ${}_a^C D_x^\alpha u(x) = u^{(m)}(x)$ and ${}_x^C D_b^\alpha u(x) = (-1)^m u^{(m)}(x)$.

The two frequently-used fractional derivatives are equivalent with exactness to an additive factor:

$${}_a^C D_x^\alpha u(x) = {}_a^{RL} D_x^\alpha u(x) - \sum_{l=0}^{m-1} \frac{u^{(l)}(a)}{\Gamma(l+1-\alpha)} (x-a)^{l-\alpha}, \quad (2.5)$$

$${}_x^C D_b^\alpha u(x) = {}_x^{RL} D_b^\alpha u(x) - \sum_{l=0}^{m-1} \frac{u^{(l)}(b)}{\Gamma(l+1-\alpha)} (b-x)^{l-\alpha}. \quad (2.6)$$

In addition, we easily realize the following properties:

$${}_a^C D_x^\alpha C = 0, \quad (2.7)$$

$${}_a J_x^{\alpha_1} {}_a J_x^{\alpha_2} u(x) = {}_a J_x^{\alpha_2} {}_a J_x^{\alpha_1} u(x) = {}_a J_x^{\alpha_1+\alpha_2} u(x), \quad (2.8)$$

$${}_a^C D_x^\alpha (x-a)^\beta = {}_a^{RL} D_x^\alpha (x-a)^\beta = \frac{\Gamma(1+\beta)}{\Gamma(1+\beta-\alpha)} (x-a)^{\beta-\alpha}, \quad (2.9)$$

where C is a constant and $\beta > [\alpha] + 1$ with $[x]$ being the ceiling function, which outputs the smallest integer greater than or equal to x . Another point need to be noticed is that these properties are also true for the right-side fractional calculus. For more details, we refer the readers to [25] for deeper insights.

2.2. Radial basis functions

The RBFs provide an effective tool for the interpolation of scattered data in multi-dimensional domains. Since they only take the space distance as independent variable, as compared to the traditional basis function defined along coordinates, RBFs have the advantages of concise form, dimension-independent and isotropic properties. In particular, in the application of solving high-dimensional PDEs, the RBFs interpolation shows great flexibility in creating collocating schemes. The numerical methods constructed by RBFs not only have the simplicity in the implementation,

but also avoid the tedious mesh generation and thereby reduce the pre-processing process of algorithms. Let $\|\cdot\|$ be the Euclidean norm and $r = \|\cdot\|$, then the commonly used RBFs are given in Table 1 and c is the shape parameter.

Letting $\mathbf{x} = (x_1, x_2, \dots, x_d)$, $\{\mathbf{x}_i\}_{i=0}^M \in \Omega \subset \mathbb{R}^d$, the approximation of $u(\mathbf{x})$ can be written as a weighted sum of RBFs in the form:

$$u(\mathbf{x}) \approx \sum_{i=0}^M \lambda_i \varphi(r_i) + \sum_{q=1}^Q \mu_q p_q(\mathbf{x}), \quad \mathbf{x} \in \Omega, \quad (2.10)$$

where $d = 1, 2, 3$, $Q = (n+d-1)!/(d!(n-1)!)$, $\{\lambda_i\}_{i=0}^M$, $\{\mu_q\}_{q=1}^Q$ are unknown weights, $\{p_q(\mathbf{x})\}_{q=1}^Q$ are the basis functions of the polynomial space of degree at most $n-1$, and $\{\varphi(r_i)\}_{i=0}^M$ are RBFs, in which, $r_i = \|\mathbf{x} - \mathbf{x}_i\|$. To ensure that the interpolant properly behave at infinity, the above equations are augmented by

$$\sum_{i=0}^M \lambda_i p_q(\mathbf{x}_i) = 0, \quad q = 1, 2, \dots, Q. \quad (2.11)$$

Putting Eqs. (2.10)-(2.11) in matrix-vector form reaches to

$$\begin{bmatrix} \mathbf{A} & \mathbf{B}^T \\ \mathbf{B} & \mathbf{0} \end{bmatrix} \begin{pmatrix} \boldsymbol{\lambda} \\ \boldsymbol{\mu} \end{pmatrix} = \begin{pmatrix} \mathbf{u} \\ \mathbf{0} \end{pmatrix}, \quad (2.12)$$

where the matrix elements for $[\mathbf{A}]$ are $\varphi(r_{ij})$ and for $[\mathbf{B}]$ are $p_j(\mathbf{x}_i)$ with $r_{ij} = \|\mathbf{x}_j - \mathbf{x}_i\|$. $\boldsymbol{\lambda}$, $\boldsymbol{\mu}$, and \mathbf{u} are column vectors and the vector elements for them are λ_i , μ_i , and $u(\mathbf{x}_i)$, respectively.

Table 1: Some commonly used RBFs.

Name	RBF
Multiquadric (MQ)	$\varphi(r) = (r^2 + c^2)^{1/2}$, $c > 0$
Inverse Multiquadric (IMQ)	$\varphi(r) = 1/(r^2 + c^2)^{1/2}$, $c > 0$
Inverse Quadratic (IQ)	$\varphi(r) = 1/(r^2 + c^2)$, $c > 0$
Gaussian (GA)	$\varphi(r) = e^{-r^2/c^2}$, $c > 0$
Polyharmonic Spline (PS)	$\varphi(r) = (-1)^{s+1} r^{2s} \ln r$, $s \in \mathbb{Z}^+$

Definition 2.4. A function is completely monotonic if and only if $(-1)^\ell f^{(\ell)}(r) \geq 0$ for $\ell = 0, 1, 2, \dots$, and $r \geq 0$.

Theorem 2.1. [9] Let an univariate function $\psi(r) \in C^\infty[0, +\infty)$ be such that ψ is completely monotonic, but not a constant. Suppose further that $\psi(0) \geq 0$. Then the interpolation matrix $[\mathbf{A}]$ of the basis function $\varphi(r) = \psi(r^2)$ is positive definite.

The Eq. (2.12) is solved for $\{\lambda_i\}_{i=0}^M$, $\{\mu_q\}_{q=1}^Q$. According to Theorem 2.1, Inverse Multiquadrics, Inverse Quadratics, and Gaussians are positive definite so that their interpolation matrices $[\mathbf{A}]$ invertible. Multiquadrics do not fulfill the above theorem and are actually conditionally positive definite under $Q \geq 1$. Therefore, the polynomial term on the right-side of Eq. (2.10) can be removed for Inverse Multiquadrics, Inverse Quadratics, and Gaussians while it is indispensable to Multiquadrics to maintain the well-posedness of the resulting algebraic system.

3. The DQ approximation of fractional derivatives

In this section, we derive a new class of DQ formulas for fractional derivatives by using RBFs as the trial functions. The DQ formula employs the weighted sum of function values at discrete nodes to approximate the partial derivatives with regard to an independent variable. Supposing $u(\mathbf{x}) \in C^m(\Omega)$, $m \in \mathbb{Z}^+$, we have the DQ formula [43]:

$$u_{x_i}^{(m)}(\mathbf{x}_i, t) \approx \sum_{j=0}^M w_{ij}^m u(\mathbf{x}_j, t), \quad i = 0, 1, \dots, M, \quad (3.13)$$

where $1 \leq l \leq d$, $w_{ij}^{m_l}$, $i, j = 0, 1, \dots, M$, are the weighted coefficients. Realizing the essence of DQ formula, we propose the following DQ formulas to the left-hand fractional derivatives:

$$\frac{\partial_+^\alpha u(\mathbf{x}_i, t)}{\partial x_{l,+}^\alpha} \approx \sum_{j=0}^M w_{ij}^{\alpha_l^+} u(\mathbf{x}_j, t), \quad i = 0, 1, \dots, M, \quad (3.14)$$

where $w_{ij}^{\alpha_l^+}$, $i, j = 0, 1, \dots, M$, are the related weighted coefficients, which satisfy

$$\frac{\partial_+^\alpha \phi_k(\mathbf{x}_i)}{\partial x_{l,+}^\alpha} = \sum_{j=0}^M w_{ij}^{\alpha_l^+} \phi_k(\mathbf{x}_j), \quad i, k = 0, 1, \dots, M, \quad (3.15)$$

with $\{\phi_k(\mathbf{x})\}_{k=0}^M$ being the trial functions. The values of the weighted coefficients are computed by solving Eqs. (3.15) via reforming them in matrix-vector form in advance. In the same way, we can extend the above DQ formulas to the right-side fractional derivatives with regard to the variables x , y and z .

Most notable is the truth that the DQ formulas (3.14) are convergent to the fractional derivative since fractional derivative operators are all linear. In the linear space V_h , spanned by the basis functions $\{\phi_k(\mathbf{x})\}_{k=0}^M$, any function in V_h can be approximated by a weighted sum of $\{\phi_k(\mathbf{x})\}_{k=0}^M$. We need to calculate the unknown weights and the values of fractional derivatives at collocating nodes by acting the fractional derivative operators on both sides of the interpolation of this function. However, given the assumption (3.15), this function can be represented by a weighted sum of functional values via the same weighted coefficients. More precisely, if $u(\mathbf{x}, t) \approx \sum_{k=0}^M \delta_k(t) \phi_k(\mathbf{x})$, $\mathbf{x} \in \Omega$, and the weighted coefficients fulfill Eqs. (3.15), then for $\frac{\partial_+^\alpha u(\mathbf{x}, t)}{\partial x_{l,+}^\alpha}$, we realize

$$\frac{\partial_+^\alpha u(\mathbf{x}_i, t)}{\partial x_{l,+}^\alpha} \approx \sum_{k=0}^M \delta_k(t) \frac{\partial_+^\alpha \phi_k(\mathbf{x}_i)}{\partial x_{l,+}^\alpha} = \sum_{k=0}^M \delta_k(t) \sum_{j=0}^M w_{ij}^{\alpha_l^+} \phi_k(\mathbf{x}_j) \approx \sum_{j=0}^M w_{ij}^{\alpha_l^+} u(\mathbf{x}_j, t) \quad (3.16)$$

via the linearity of fractional derivatives, which guarantees the convergence of DQ formulas. Moreover, this convergent result is exactly true for the right-side fractional derivatives with regard to the other variables. Consequently, the values of fractional derivatives can be obtained without calculating the weights $\{\delta_k(t)\}_{k=0}^M$.

The determination of weighted coefficients also comprise a major part of DQ methods. In the sequel, we show how to use the aforementioned RBFs to compute their values. It should be noted that for Inverse Multiquadrics, Inverse Quadratics and Gaussians, their interpolation matrices invertible. Hence, ignoring the polynomial terms on the right-side of RBFs interpolation (2.10) and substitute $\phi_k(\mathbf{x}_i) = \varphi(r_{ki})$ into Eq. (3.15), we obtain the weighted coefficients by solving the resulting algebraic systems for each node \mathbf{x}_i . As for Multiquadrics, we prefer to

$$u(\mathbf{x}, t) \approx \sum_{i=0}^M \lambda_i(t) \varphi(r_i) + \mu_1(t). \quad (3.17)$$

To make the problem well posed, one more equation is required. From Eq. (2.11), it follows that $\lambda_0(t) = -\sum_{i=1}^M \lambda_i(t)$, which yields

$$u(\mathbf{x}, t) \approx \sum_{i=1}^M \lambda_i(t) \{\varphi(r_i) - \varphi(r_0)\} + \mu_1(t).$$

By careful observation, we consider $\phi_0(\mathbf{x}) = 1$, $\phi_i(\mathbf{x}) = \varphi(r_i) - \varphi(r_0)$, $i = 1, 2, \dots, M$, as trial functions. Referring to the above discussion and ${}_a^C D_x^{\alpha_l} 1 = 0$, we obtain the linear systems of equations $\mathbf{M} \mathbf{w}_i^{\alpha_l^+} = \mathbf{R}_i$, $i = 0, 1, \dots, M$, where

$$\mathbf{M} = \begin{pmatrix} 1 & 1 & \cdots & 1 \\ \varphi(r_{10}) - \varphi(r_{00}) & \varphi(r_{11}) - \varphi(r_{01}) & \cdots & \varphi(r_{1M}) - \varphi(r_{0M}) \\ \vdots & \vdots & & \vdots \\ \varphi(r_{M0}) - \varphi(r_{00}) & \varphi(r_{M1}) - \varphi(r_{01}) & \cdots & \varphi(r_{MM}) - \varphi(r_{0M}) \end{pmatrix},$$

$$\mathbf{w}_i^{\alpha_i^+} = \begin{pmatrix} w_{i0}^{\alpha_i^+} \\ w_{i1}^{\alpha_i^+} \\ \vdots \\ w_{iM}^{\alpha_i^+} \end{pmatrix}, \quad \mathbf{R}_i = \begin{pmatrix} 0 \\ \frac{\partial_+^\alpha \varphi(r_{1i})}{\partial x_{i,+}^\alpha} - \frac{\partial_+^\alpha \varphi(r_{0i})}{\partial x_{i,+}^\alpha} \\ \vdots \\ \frac{\partial_+^\alpha \varphi(r_{Mi})}{\partial x_{i,+}^\alpha} - \frac{\partial_+^\alpha \varphi(r_{0i})}{\partial x_{i,+}^\alpha} \end{pmatrix}.$$

For each node \mathbf{x}_i , the values of weighted coefficients are finally determined by $\mathbf{w}_i^{\alpha_i^+} = \mathbf{M}^{-1} \mathbf{R}_i$.

Remarks 3.1. Like most of RBFs-based methods, a problem has to be faced for the RBFs-based DQ formula is the selection of the values of shape parameters. One can dramatically reduce error by adjusting the shape parameter to make the interpolator optimally flat. This improvement in accuracy is accomplished without reducing the fill distance of nodes, but need to increase the condition number of \mathbf{M} . Actually, this is still a open problem and mathematical theories study on its optimal value is abundant. We can choose it on the basis of some empirical formulas.

4. The description of RBFs-based DQ method

4.1. Discretization of time-fractional derivative

In this subsection, we introduce a family of high-order difference schemes to discretize the fractional derivative in time. To this end, we define a time lattice $t_n = n\tau$, $n = 0, 1, \dots, N$, $T = \tau N$, $N \in \mathbb{Z}^+$ and review the relationship between Caputo and Riemann-Liouville fractional derivatives:

$${}_0^C D_t^\theta u(\mathbf{x}, t) = {}_0^{RL} D_t^\theta u(\mathbf{x}, t) - \sum_{l=0}^{m-1} \frac{u_t^{(l)}(\mathbf{x}, 0) t^{l-\theta}}{\Gamma(l+1-\theta)}, \quad (4.18)$$

where $m-1 < \theta < m$, $m \in \mathbb{Z}^+$. Using the property (2.9), we obtain a family of high-order schemes for Caputo derivative by applying the Lubich's difference operators $\mathcal{L}_q^\theta u(\mathbf{x}, t_n) = \frac{1}{\tau^\theta} \sum_{k=0}^n \omega_k^{q,\theta} u(\mathbf{x}, t_{n-k})$, $q = 1, 2, 3, 4, 5$, to discretize the Riemann-Liouville derivatives on the right-side of Eq. (4.18), which reads

$${}_0^C D_t^\theta u(\mathbf{x}, t_n) \approx \frac{1}{\tau^\theta} \sum_{k=0}^n \omega_k^{q,\theta} u(\mathbf{x}, t_{n-k}) - \frac{1}{\tau^\theta} \sum_{l=0}^{m-1} \sum_{k=0}^n \frac{\omega_k^{q,\theta} u_t^{(l)}(\mathbf{x}, 0) t_{n-k}^l}{l!}, \quad (4.19)$$

where $\{\omega_k^{q,\theta}\}_{k=0}^n$ are the discrete coefficients [8]. For example, when $q = 1$, we have $\omega_k^{1,\theta} = (-1)^k \binom{\theta}{k} = \frac{\Gamma(k-\theta)}{\Gamma(-\theta)\Gamma(k+1)}$, $k = 0, 1, 2, \dots$, and when $q = 3$, we have

$$\omega_k^{3,\theta} = \left(\frac{11}{6}\right)^\theta \sum_{p=0}^k \sum_{q=0}^p \mu^q \bar{\mu}^{p-q} \omega_q^{1,\theta} \omega_{p-q}^{1,\theta} \omega_{k-p}^{1,\theta}, \quad (4.20)$$

where $\mu = \frac{4}{7+\sqrt{391}}$, $\bar{\mu} = \frac{4}{7-\sqrt{391}}$ and i denotes the imaginary unit.

Lemma 4.1. The coefficients $\omega_k^{1,\theta}$ satisfy the following properties

- (i) $\omega_0^{1,\theta} = 1$, $\omega_k^{1,\theta} < 0$, $\sum_{k=0}^{\infty} \omega_k^{1,\theta} = 0$, $\sum_{k=0}^{n-1} \omega_k^{1,\theta} > 0$, $\forall k = 1, 2, \dots$,
- (ii) $\omega_0^{1,\theta} = 1$, $\omega_k^{1,\theta} = \left(1 - \frac{\theta+1}{k}\right) \omega_{k-1}^{1,\theta}$, $\forall k = 1, 2, \dots$

Lemma 4.2. [8] Assume that $u(\mathbf{x}, t)$, ${}_0^{RL} D_t^{\theta+q} u(\mathbf{x}, t)$ and their Fourier transforms belong to $L^1(\mathbb{R})$ with regard to t , then the Lubich's difference operators satisfy

$${}_0^{RL} D_t^\theta u(\mathbf{x}, t_n) = \mathcal{L}_q^\theta u(\mathbf{x}, t_n) + \mathcal{O}(\tau^q). \quad (4.21)$$

Theorem 4.1. Assume that $u(\mathbf{x}, t)$ with $\theta > 0$ is smooth enough with regard to t , then we have

$${}_0^C D_t^\theta u(\mathbf{x}, t_n) = \mathcal{A}_q^\theta u(\mathbf{x}, t_n) + \mathcal{O}(\tau^q), \quad (4.22)$$

where

$$\mathcal{A}_q^\theta u(\mathbf{x}, t_n) = \frac{1}{\tau^\theta} \sum_{k=0}^n \omega_k^{q,\theta} u(\mathbf{x}, t_{n-k}) - \frac{1}{\tau^\theta} \sum_{l=0}^{m-1} \sum_{k=0}^n \frac{\omega_k^{q,\theta} u_t^{(l)}(\mathbf{x}, 0) t_{n-k}^l}{l!}.$$

The proof is trivial by following Lemma 4.2. Applying the operator \mathcal{A}_q^θ to the multi-term fractional derivative operator and set $0 < \theta \leq 1$, we finally obtain

$$\begin{aligned} P_{\theta_1, \theta_2, \dots, \theta_s}({}_0^C \mathcal{D}_t) u(\mathbf{x}, t_n) &= a_{10} {}_0^C D_t^{\theta_1} u(\mathbf{x}, t_n) + a_{20} {}_0^C D_t^{\theta_2} u(\mathbf{x}, t_n) + \dots + a_{s0} {}_0^C D_t^{\theta_s} u(\mathbf{x}, t_n) \\ &= a_1 \mathcal{A}_q^{\theta_1} u(\mathbf{x}, t_n) + a_2 \mathcal{A}_q^{\theta_2} u(\mathbf{x}, t_n) + \dots + a_s \mathcal{A}_q^{\theta_s} u(\mathbf{x}, t_n) + \mathcal{O}(\tau^q) \\ &= \sum_{r=1}^s a_r \mathcal{A}_q^{\theta_r} u(\mathbf{x}, t_n) + \mathcal{O}(\tau^q) \\ &= \sum_{r=1}^s \frac{a_r}{\tau^{\theta_r}} \sum_{k=0}^{n-1} \omega_k^{q,\theta_r} u(\mathbf{x}, t_{n-k}) - \sum_{r=1}^s \frac{a_r}{\tau^{\theta_r}} \sum_{k=0}^{n-1} \omega_k^{q,\theta_r} u(\mathbf{x}, 0) + \mathcal{O}(\tau^q). \end{aligned} \quad (4.23)$$

One last thing should be hinted at is that the schemes in Eq. (4.23) degenerate into the classical backward difference schemes when \mathcal{A}_q^θ is only a single-term fractional derivative operator with $\theta = 1$.

4.2. Fully discrete RBFs-based DQ scheme

In this subsection, we develop a fully discrete DQ scheme for the multi-term TSFPDEs, which utilizes the operator \mathcal{A}_q^θ to treat the Caputo derivative in time and the RBFs-based DQ formulas to approximate the fractional derivatives in space. For simplicity, letting $\mathbf{x} = (x_1, x_2, \dots, x_d)$, $\Omega \subset \mathbb{R}^d$, we put Eqs. (1.1)-(1.2) in a unified form:

$$\begin{cases} P_{\theta_1, \theta_2, \dots, \theta_s}({}_0^C \mathcal{D}_t) u(\mathbf{x}, t) - \sum_{l=1}^d \varepsilon_{\alpha_l}^+(\mathbf{x}) \frac{\partial^{\alpha_l} u(\mathbf{x}, t)}{\partial x_{l,+}^{\alpha_l}} - \sum_{l=1}^d \varepsilon_{\alpha_l}^-(\mathbf{x}) \frac{\partial^{\alpha_l} u(\mathbf{x}, t)}{\partial x_{l,-}^{\alpha_l}} = f(\mathbf{x}, t), & (\mathbf{x}; t) \in \Omega \times (0, T], \\ u(\mathbf{x}, 0) = u_0(\mathbf{x}), & \mathbf{x} \in \Omega, \\ u(\mathbf{x}, t) = g(\mathbf{x}, t), & (\mathbf{x}; t) \in \partial\Omega \times (0, T], \end{cases} \quad (4.24)$$

where $0 < \theta_1, \theta_2, \dots, \theta_s \leq 1$, $1 < \alpha_l \leq 2$ and $l = 1, 2, \dots, d$.

Let $\{\mathbf{x}_i\}_{i=0}^M$ be a set of nodes in $\Omega \subset \mathbb{R}^d$. Replacing the space-fractional derivatives by RBFs-based DQ formulas, we have the multi-term fractional ODEs as follows:

$$P_{\theta_1, \theta_2, \dots, \theta_s}({}_0^C \mathcal{D}_t) u(\mathbf{x}_i, t) - \sum_{l=1}^d \varepsilon_{\alpha_l}^+(\mathbf{x}_i) \sum_{j=0}^M w_{ij}^{\alpha_l^+} u(\mathbf{x}_j, t) - \sum_{l=1}^d \varepsilon_{\alpha_l}^-(\mathbf{x}_i) \sum_{j=0}^M w_{ij}^{\alpha_l^-} u(\mathbf{x}_j, t) = f(\mathbf{x}_i, t), \quad (4.25)$$

where $i = 0, 1, \dots, M$. Furthermore, using the operator \mathcal{A}_q^θ to discretize $P_{\theta_1, \theta_2, \dots, \theta_s}({}_0^C \mathcal{D}_t)$ arrives at

$$\sum_{r=1}^s a_r \mathcal{A}_q^{\theta_r} u(\mathbf{x}_i, t_n) - \sum_{l=1}^d \varepsilon_{\alpha_l}^+(\mathbf{x}_i) \sum_{j=0}^M w_{ij}^{\alpha_l^+} u(\mathbf{x}_j, t_n) - \sum_{l=1}^d \varepsilon_{\alpha_l}^-(\mathbf{x}_i) \sum_{j=0}^M w_{ij}^{\alpha_l^-} u(\mathbf{x}_j, t_n) = f(\mathbf{x}_i, t_n) + \mathcal{O}(\tau^q). \quad (4.26)$$

Ignoring $\mathcal{O}(\tau^q)$ and enforcing Eq. (4.26) exactly holds at $\{\mathbf{x}_i\}_{i=0}^M$, we obtain the fully discrete DQ scheme:

$$\begin{cases} \sum_{r=1}^s \frac{a_r \omega_0^{q,\theta_r}}{\tau^{\theta_r}} u(\mathbf{x}_i, t_n) - \sum_{l=1}^d \varepsilon_{\alpha_l}^+(\mathbf{x}_i) \sum_{j=0}^M w_{ij}^{\alpha_l^+} u(\mathbf{x}_j, t_n) - \sum_{l=1}^d \varepsilon_{\alpha_l}^-(\mathbf{x}_i) \sum_{j=0}^M w_{ij}^{\alpha_l^-} u(\mathbf{x}_j, t_n) \\ = f(\mathbf{x}_i, t_n) - \sum_{r=1}^s \frac{a_r}{\tau^{\theta_r}} \sum_{k=1}^{n-1} \omega_k^{q,\theta_r} u(\mathbf{x}_i, t_{n-k}) + \sum_{r=1}^s \frac{a_r}{\tau^{\theta_r}} \sum_{k=0}^{n-1} \omega_k^{q,\theta_r} u(\mathbf{x}_i, 0), & (\mathbf{x}_i; t_n) \in \Omega \times (0, T], \\ u(\mathbf{x}_i, 0) = u_0(\mathbf{x}_i), & \mathbf{x}_i \in \Omega, \\ u(\mathbf{x}_i, t_n) = g(\mathbf{x}_i, t_n), & (\mathbf{x}_i; t_n) \in \partial\Omega \times (0, T], \end{cases} \quad (4.27)$$

where $i = 0, 1, \dots, M$ and $n = 0, 1, \dots, N$.

For the ease of expression, we employ the notations $U_i^n = u(\mathbf{x}_i, t_n)$, $\varepsilon_{\alpha_l, i}^\pm = \varepsilon_{\alpha_l}^\pm(\mathbf{x}_i)$, $f_i^n = f(\mathbf{x}_i, t_n)$, $g_i^n = g(\mathbf{x}_i, t_n)$, and $\mathbf{U}^n, \mathbf{F}^n, \mathbf{g}^n$ are the column vectors consisting of U_i^n, f_i^n and g_i^n in the ascending order of subscript i , respectively. Also, we adopt $\varepsilon_{\alpha_l}^\pm = \text{diag}(\varepsilon_{\alpha_l, 0}^\pm, \varepsilon_{\alpha_l, 1}^\pm, \dots, \varepsilon_{\alpha_l, M}^\pm)$. Reforming Eqs. (4.27) in a matrix-vector form leads to

$$\begin{cases} \sum_{r=1}^s \frac{a_r \omega_0^{q, \theta_r}}{\tau^{\theta_r}} \mathbf{U}^n - \sum_{l=1}^d \varepsilon_{\alpha_l}^+ \mathbf{W}_{\alpha_l}^+ \mathbf{U}^n - \sum_{l=1}^d \varepsilon_{\alpha_l}^- \mathbf{W}_{\alpha_l}^- \mathbf{U}^n \\ = \mathbf{F}^n - \sum_{r=1}^s \frac{a_r}{\tau^{\theta_r}} \sum_{k=1}^{n-1} \omega_k^{q, \theta_r} \mathbf{U}^{n-k} + \sum_{r=1}^s \frac{a_r}{\tau^{\theta_r}} \sum_{k=0}^{n-1} \omega_k^{q, \theta_r} \mathbf{U}^0, \\ U_i^n = g_i^n, \quad \text{for } \mathbf{x}_i \in \partial\Omega, \end{cases} \quad (4.28)$$

where $n = 0, 1, \dots, N$ and $\mathbf{W}_{\alpha_l}^\pm$ are the weighted coefficient matrices, given by

$$\mathbf{W}_{\alpha_l}^\pm = \begin{pmatrix} w_{00}^{\alpha_l^\pm} & w_{01}^{\alpha_l^\pm} & \cdots & w_{0M}^{\alpha_l^\pm} \\ w_{10}^{\alpha_l^\pm} & w_{11}^{\alpha_l^\pm} & \cdots & w_{1M}^{\alpha_l^\pm} \\ \vdots & \vdots & \ddots & \vdots \\ w_{M0}^{\alpha_l^\pm} & w_{M1}^{\alpha_l^\pm} & \cdots & w_{MM}^{\alpha_l^\pm} \end{pmatrix}, \quad l = 1, 2, \dots, d.$$

By solving the algebraic equations resulting from the RBFs-based DQ scheme (4.28), we obtain the desirable solutions for the considered problems at each time layer. However, it should be noticed that the above scheme cannot be directly implemented in computers. Consequently, we turn our eyes to the executable form of the proposed DQ scheme (4.28) and the implementation of its algorithm. Before we do, an important problem having to be addressed is how to compute the fractional derivatives of RBFs and determine the corresponding integral paths. It is acknowledged that the fractional derivative of a general function like RBFs is quite difficult to compute. We will be engaged in this point. For a node $\mathbf{x}_i \in \Omega$ and the RBF $\varphi(r_i)$, letting $\xi = x_l - (x_l - X_{l,L})(1 + \zeta)/2$, one has

$$\frac{\partial_+^\alpha \varphi_k(r_i)}{\partial x_{l,+}^\alpha} = \frac{1}{\Gamma(2 - \alpha)} \left(\frac{x_l - X_{l,L}}{2} \right)^{2-\alpha} \int_{-1}^1 \left\{ (1 + \zeta)^{1-\alpha} \frac{\partial^2 \varphi_k(r_i|_{x_l=\xi})}{\partial \xi^2} \Big|_{\xi=x_l-(x_l-X_{l,L})(1+\zeta)/2} \right\} d\zeta, \quad (4.29)$$

where $X_{l,L} = \min\{\eta_l : (\eta_1, \eta_2, \dots, \eta_d), \eta_i = x_i, i \neq l\}$. Then, it can be tackled by Gauss-Jacobi quadrature formula [35]. The line segment along the x_l -coordinate axis from the left-side of boundary to the node \mathbf{x}_i is called the integral path, which need to be determined before the calculation of fractional derivatives.

Hereafter, we will introduce how to perform the RBFs-based DQ algorithm. Use Matlab as platform for programming and let **nodei**, **nodeb** be the index vectors of the internal and boundary nodes in Ω , respectively. For the sake of simplicity, we define $\tilde{\mathbf{U}}^n = \mathbf{U}^n(\mathbf{nodei})$, $\mathbf{I} = \text{eye}(\text{length}(\mathbf{nodeb}))$, $\tilde{\varepsilon}_{\alpha_l}^\pm = \varepsilon_{\alpha_l}^\pm(\mathbf{nodei}, \mathbf{nodei})$, $\mathbf{K}_{\alpha_l}^\pm = \mathbf{W}_{\alpha_l}^\pm(\mathbf{nodei}, \mathbf{nodei})$, $\mathbf{G}_{\alpha_l}^\pm = \mathbf{W}_{\alpha_l}^\pm(\mathbf{nodei}, \mathbf{nodeb})$, $\tilde{\mathbf{F}}^n = \mathbf{F}^n(\mathbf{nodei})$, and $\tilde{\mathbf{g}}^n = \mathbf{g}^n(\mathbf{nodeb})$. Imposing the boundary condition $U_i^n = g_i^n, \mathbf{x}_i \in \partial\Omega$, we obtain the following fully discrete RBFs-based DQ scheme

$$\begin{aligned} & \left(\sum_{r=1}^s \frac{a_r \omega_0^{q, \theta_r}}{\tau^{\theta_r}} \mathbf{I} - \sum_{l=1}^d \tilde{\varepsilon}_{\alpha_l}^+ \mathbf{K}_{\alpha_l}^+ - \sum_{l=1}^d \tilde{\varepsilon}_{\alpha_l}^- \mathbf{K}_{\alpha_l}^- \right) \tilde{\mathbf{U}}^n \\ & = \tilde{\mathbf{F}}^n - \sum_{r=1}^s \frac{a_r}{\tau^{\theta_r}} \sum_{k=1}^{n-1} \omega_k^{q, \theta_r} \tilde{\mathbf{U}}^{n-k} + \sum_{r=1}^s \frac{a_r}{\tau^{\theta_r}} \sum_{k=0}^{n-1} \omega_k^{q, \theta_r} \tilde{\mathbf{U}}^0 \\ & + \sum_{p=1}^{Q^*} \sum_{l=1}^d \tilde{\varepsilon}_{\alpha_l}^+ \tilde{\mathbf{g}}^n(p) \mathbf{G}_{\alpha_l}^+(\cdot, p) + \sum_{p=1}^{Q^*} \sum_{l=1}^d \tilde{\varepsilon}_{\alpha_l}^- \tilde{\mathbf{g}}^n(p) \mathbf{G}_{\alpha_l}^-(\cdot, p), \end{aligned} \quad (4.30)$$

which can be directly implemented, where $Q^* = \text{length}(\mathbf{nodei})$, $\mathbf{U}^n(\mathbf{nodei})$ are the unknown vectors which yet to be determined. A detailed implementation of the algorithm for the DQ scheme (4.30) is presented as follow:

Algorithm 1: Fully discrete RBFs-based DQ algorithm

Data: $\alpha_l, \theta_r, a_r, s, q, d, \tau, M, \{t_n\}_{n=0}^N$, and $\{\mathbf{x}_i\}_{i=0}^M$
Result: the numerical solution \mathbf{U} at all time levels

- 1 $i \leftarrow 0, r \leftarrow 1, n \leftarrow 1, k \leftarrow 1, p \leftarrow 1$;
- 2 get internal and boundary nodes and the corresponding index vectors **nodei**, **nodeb**;
- 3 initialize the matrices $\mathbf{U}, \mathbf{W}_{\alpha_l}^\pm$ and form $\boldsymbol{\varepsilon}_{\alpha_l}^\pm, \mathbf{M}$, and $\mathbf{C} \leftarrow \text{zeros}(s, N+1)$;
- 4 **while** $0 \leq i \leq M$ **do**
- 5 determine the line segment along coordinate axis for \mathbf{x}_i ;
- 6 compute the fractional derivatives of RBFs by (4.29) and assemble \mathbf{R}_i ;
- 7 determine the weighted coefficients $w_{ij}^{\alpha_l^\pm}$ and set $\mathbf{w}_i^{\alpha_l^\pm} \leftarrow \mathbf{M}^{-1} \mathbf{R}_i$;
- 8 $\mathbf{W}_{\alpha_l}^\pm(i+1, :) \leftarrow (\mathbf{w}_i^{\alpha_l^\pm})^T$; $i \leftarrow i+1$;
- 9 **end**
- 10 get $\tilde{\boldsymbol{\varepsilon}}_{\alpha_l}^\pm, \mathbf{K}_{\alpha_l}^\pm, \mathbf{G}_{\alpha_l}^\pm, \tilde{\mathbf{F}}^n, \tilde{\mathbf{g}}^n$, and $\mathbf{I} \leftarrow \text{eye}(\text{length}(\mathbf{nodei}))$;
- 11 **while** $1 \leq r \leq s$ **do**
- 12 generate the discrete coefficients ω_k^{q, θ_r} by Lemma 4.1 and the formulas (4.20), $k = 0, 1, 2, \dots$;
- 13 $\mathbf{C}(r, k+1) \leftarrow a_r \omega_k^{q, \theta_r} / \tau^{\theta_r}$; $r \leftarrow r+1$;
- 14 **end**
- 15 $\mathbf{c} \leftarrow \text{sum}(\mathbf{C})$, $\mathbf{U}(:, 1) = \mathbf{U}^0$;
- 16 $\mathbf{K} \leftarrow \mathbf{c}(1)\mathbf{I} - \sum_{l=1}^d \tilde{\boldsymbol{\varepsilon}}_{\alpha_l}^+ \mathbf{K}_{\alpha_l}^+ - \sum_{l=1}^d \tilde{\boldsymbol{\varepsilon}}_{\alpha_l}^- \mathbf{K}_{\alpha_l}^-$, $Q^* \leftarrow \text{length}(\mathbf{nodei})$;
- 17 **while** $1 \leq n \leq N$ **do**
- 18 $\mathbf{U}^* \leftarrow \mathbf{c}(1)\mathbf{U}(:, 1)$; $\mathbf{U}^{**} \leftarrow \text{zeros}(\text{length}(\mathbf{nodei}), 1)$;
- 19 **while** $1 \leq k \leq n-1$ **do**
- 20 $\mathbf{U}^* \leftarrow \mathbf{U}^* + \mathbf{c}(k+1)\mathbf{U}(:, 1)$; $\mathbf{U}^{**} \leftarrow \mathbf{U}^{**} + \mathbf{c}(k+1)\mathbf{U}(:, n-k+1)$;
- 21 $k \leftarrow k+1$;
- 22 **end**
- 23 $\mathbf{P}^n \leftarrow \mathbf{U}^* - \mathbf{U}^{**} + \tilde{\mathbf{F}}^n + \sum_{p=1}^{Q^*} \sum_{l=1}^d \tilde{\boldsymbol{\varepsilon}}_{\alpha_l}^+ \tilde{\mathbf{g}}^n(p) \mathbf{G}_{\alpha_l}^+(:, p) + \sum_{p=1}^{Q^*} \sum_{l=1}^d \sum_{l=1}^d \tilde{\boldsymbol{\varepsilon}}_{\alpha_l}^- \tilde{\mathbf{g}}^n(p) \mathbf{G}_{\alpha_l}^-(p)$;
- 24 solve $\mathbf{K} \tilde{\mathbf{U}}^n = \mathbf{P}^n$ and set $\tilde{\mathbf{U}}^n \leftarrow \mathbf{K} \setminus \mathbf{P}^n$;
- 25 $\mathbf{U}(\mathbf{nodei}, n+1) \leftarrow \tilde{\mathbf{U}}^n$, $\mathbf{U}(\mathbf{nodeb}, n+1) \leftarrow \tilde{\mathbf{g}}^n$, $n \leftarrow n+1$;
- 26 **end**
- 27 return \mathbf{U}

5. Illustrative examples

Let u_i^n, U_i^n be the analytical and numerical solutions at the time level n . Denoting

$$\|u - U\|_{L^2} = \left[h^* \sum_{i=0}^M (u_i^n - U_i^n)^2 \right]^{\frac{1}{2}}, \quad h^* = \frac{1}{M+1},$$

$$\|u - U\|_{L^\infty} = \max_{0 \leq i \leq M} |u_i^n - U_i^n|,$$

some illustrative examples will be performed to reveal the validity and convergence of the proposed RBFs-based DQ method on different domains. We test our codes by choosing the values of the shape parameters with reference to the formula $c = \nu/(M+1)^{\sigma/4}$, where $\nu > 0$, $\sigma \in \mathbb{Z}^+$, and solve all one-dimensional problems on the nodal distribution

$x_i = (1 - \cos \frac{i\pi}{M})(b - a)/2 + a, i = 0, 1, \dots, M$, when $\Omega = [a, b]$. We compute the convergent rates by

$$Cov. rate = \begin{cases} \frac{\log_2(\|u - U\|_{L^v} / \|u - U\|_{L^v}^*)}{\log_2(\tau_2 / \tau_1)}, & \text{in time,} \\ \frac{\log_2(\|u - U\|_{L^v} / \|u - U\|_{L^v}^*)}{\log_2(M_2 / M_1)}, & \text{in space,} \end{cases}$$

where $v = 2, \infty, \tau_1, \tau_2, M_1, M_2$ are the temporal stepsizes and nodal parameters, $\|u - U\|_{L^v}, \|u - U\|_{L^v}^*$ are the numerical errors, which correspond to τ_1, M_1 and τ_2, M_2 , respectively. τ_1, τ_2, M_1, M_2 should satisfy the conditions $\tau_1 \neq \tau_2, M_1 \neq M_2$. We numerically study the advantages in convergent accuracy of the proposed RBFs-based DQ method in time and space by comparing with FD and FE methods. According to the foregoing analysis, we anticipate the errors yielded by the DQ method would show a gradual decline as M increases and the convergent rate in time would strictly be q as τ decreases. Moreover, all the numerical tests are carried out by MATLAB R2014a on a personal PC with WIN 7 Pro., AMD Athlon(tm) II x2 250 3.00 GHz Processor and 4 GB DDR3 RAM.

5.1. One-dimensional problems

Example 6.1. To test the validity of the DQ formula, we discretize the left-side fractional derivative ${}_{-1}^C D_x^\alpha (x + 1)^3$ on $[-1, 1]$ by Grünwald-Letnikov (GL) difference operator and DQ formula, in which case, one has

$${}_{-1}^C D_x^\alpha (x + 1)^3 = \frac{6(x + 1)^{3-\alpha}}{\Gamma(4 - \alpha)}.$$

We choose $\alpha = 1.5$ and Inverse Multiquadrics as the trial functions with the free parameters $\nu = 1.3$ and $\sigma = 1$. The comparison of numerical errors and convergent rates for these two methods are shown in Table 2. It can be seen from this table that the convergent rates of GL-operator are strictly 1, while the convergent rates of DQ formula are much higher than GL-operator and the errors of DQ formula are much less than GL-operator. Thus, we come to the conclusion that our DQ formulas are effective and more efficient than GL-operator.

Table 2: The comparison of errors for GL-operator and DQ formula when $\alpha = 1.5$.

M	GL-operator		DQ formula	
	$\ u - U\ _{L^2}$	Cov. rate	$\ u - U\ _{L^2}$	Cov. rate
10	3.1748e-01	-	5.4602e-01	-
15	2.1632e-01	0.95	8.7341e-02	4.52
20	1.6399e-01	0.96	2.3303e-02	4.59
25	1.3203e-01	0.97	6.8577e-03	5.48

Example 6.2. Consider the one-dimensional multi-term TSFDE:

$$\begin{cases} \sum_{r=1}^4 a_{r0} {}^C D_t^{\theta_r} u(x, t) - \frac{\partial_x^\alpha u(x, t)}{\partial x_+^\alpha} = \sum_{r=1}^4 \frac{120 a_r t^{5-\theta_r} x^4}{\Gamma(6 - \theta_r)} - \frac{24 t^5 x^{4-\alpha}}{\Gamma(5 - \alpha)}, & (x, t) \in [0, 1] \times (0, T], \\ u(x, 0) = 0, & x \in [0, 1], \\ u(0, t) = 0, & u(1, t) = t^5, t \in (0, T], \end{cases} \quad (5.31)$$

with $a_1 = a_2 = a_3 = a_4 = 1, \theta_1 = 0.3, \theta_2 = 0.5, \theta_3 = 0.7, \theta_4 = 0.9$ and $\alpha = 1.2$.

The analytical solution is $u(x, t) = t^5 x^4$. Using Multiquadrics and Inverse Quadratics as the trial functions and choosing the corresponding free parameters by $\nu = 0.1, \sigma = 1$ and $\nu = 0.3, \sigma = 1$, respectively, the convergent results in space at $t = 0.5$ with $q = 1, \tau = 5.0 \times 10^{-5}$ are listed in Table 3. The comparison of numerical, analytical solutions and the absolute error distribution yielded by IQ-based DQ method at $t = 0.5$ when $M = 25$ are plotted in Fig. 1. As expected, we obviously see that the errors are quite small and the convergent rates are almost up to 4, which implies

that the proposed DQ method achieves high accuracy by using a small number of nodes. The results in the figure show the good agreement between the numerical and analytical solutions, and the error reaches its peak at the nodes where the analytical solution changes dramatically. Besides, MQ-based DQ method obtains better numerical solutions than IQ-based DQ method for this problem, while the relation of magnitude of the associated convergent rates for these two methods are completely opposite. Furthermore, we examine the convergent rates of MQ-based DQ method in time with different q . For this purpose, retaking $\nu = 0.15$, $\sigma = 1$, $q = 1, 2, 3, 4$, and $M = 50$, the numerical errors and corresponding convergent rates at $t = 0.5$ are all shown in Table 4. From the data of this table, we observe that the convergent rates of our method are nearly $\mathcal{O}(\tau^q)$ in time, which is basically what we anticipated in theory.

Table 3: The convergent results at $t = 0.5$ with $q = 1$, $\tau = 5.0 \times 10^{-5}$ and different M for Example 6.2.

M	MQ-based DQ method		IQ-based DQ method,	
	$\ u - U\ _{L^2}$	Cov. rate	$\ u - U\ _{L^2}$	Cov. rate
10	6.7983e-05	-	1.3132e-04	-
15	1.7258e-05	3.38	3.1071e-05	3.55
20	6.5139e-06	3.39	9.2979e-06	4.19
25	2.9562e-06	3.54	3.3970e-06	4.51

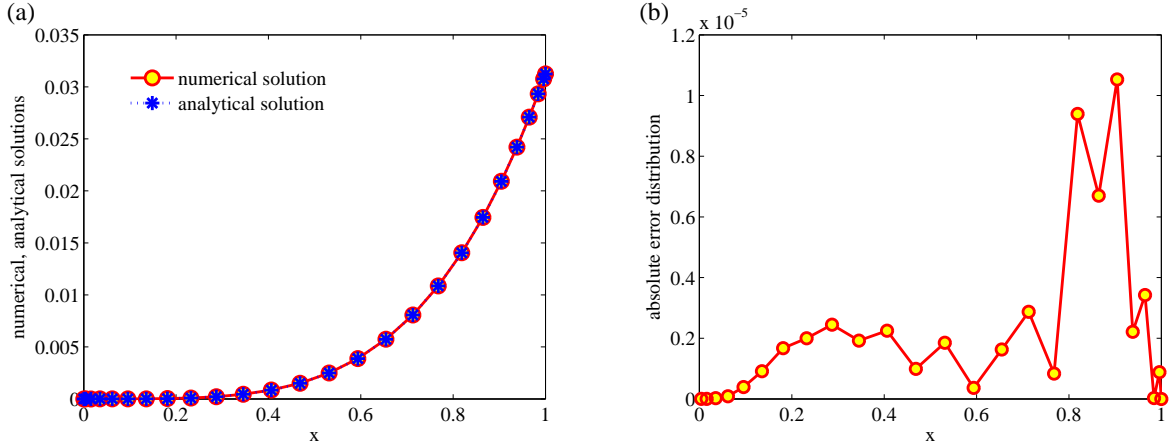


Figure 1: The comparison of numerical, analytical solutions and the absolute error distribution of IQ-based DQ method at $t = 0.5$.

5.2. Two-dimensional problems

Example 6.3. Consider the two-dimensional single-term TSFPDE:

$$\begin{cases}
 {}^C_0 D_t^\theta u(x, y, t) + \frac{1}{2 \cos(\alpha\pi/2)} \left(\frac{\partial_+^\alpha u(x, y, t)}{\partial x_+^\alpha} + \frac{\partial_-^\alpha u(x, y, t)}{\partial x_-^\alpha} \right) \\
 + \frac{1}{2 \cos(\beta\pi/2)} \left(\frac{\partial_+^\beta u(x, y, t)}{\partial y_+^\beta} + \frac{\partial_-^\beta u(x, y, t)}{\partial y_-^\beta} \right) = f(x, y, t), & (x, y, t) \in \Omega \times (0, T], \\
 u(x, y, 0) = x^2(1-x)^2y^2(1-y)^2, & (x, y) \in \Omega, \\
 u(x, y, t) = 0, & (x, y, t) \in \partial\Omega \times (0, T],
 \end{cases} \quad (5.32)$$

Table 4: The convergent results at $t = 0.5$ of MQ-based DQ method with different q , τ and $M = 50$ for Example 6.2.

	τ	$\ u - U\ _{L^2}$	Cov. rate	$\ u - U\ _{L^\infty}$	Cov. rate
$q = 1$	1/10	2.4414e-03	-	5.0450e-03	-
	1/20	1.2432e-03	0.97	2.6025e-03	0.96
	1/40	6.2677e-04	0.99	1.3202e-03	0.98
	1/80	3.1463e-04	0.99	6.6470e-04	0.99
$q = 2$	1/10	8.5486e-04	-	1.7887e-03	-
	1/20	2.5813e-04	1.73	5.4164e-04	1.72
	1/40	7.1272e-05	1.86	1.4945e-04	1.86
	1/80	1.8741e-05	1.93	3.9271e-05	1.93
$q = 3$	1/10	3.2489e-04	-	6.7717e-04	-
	1/20	5.2081e-05	2.64	1.0742e-04	2.66
	1/40	7.2778e-06	2.84	1.4941e-05	2.85
	1/80	9.6000e-07	2.92	1.9623e-06	2.93
$q = 4$	1/10	1.0892e-04	-	2.2404e-04	-
	1/20	7.8556e-06	3.79	1.5722e-05	3.83
	1/40	5.2432e-07	3.91	1.0391e-06	3.92
	1/80	3.9482e-08	3.73	1.1705e-07	3.15

on the square domain with $\Omega = [0, 1] \times [0, 1]$, $\alpha = \beta = 1.6$ and the source term

$$\begin{aligned}
 f(x, y, t) = & \frac{2t^{2-\theta}}{\Gamma(3-\theta)} x^2(1-x)^2 y^2(1-y)^2 \\
 & + \frac{(1+t^2)y^2(1-y)^2}{\cos(\alpha\pi/2)} \left\{ \frac{x^{2-\alpha} + (1-x)^{2-\alpha}}{\Gamma(3-\alpha)} - \frac{6(x^{3-\alpha} + (1-x)^{3-\alpha})}{\Gamma(4-\alpha)} + \frac{12(x^{4-\alpha} + (1-x)^{4-\alpha})}{\Gamma(5-\alpha)} \right\} \\
 & + \frac{(1+t^2)x^2(1-x)^2}{\cos(\beta\pi/2)} \left\{ \frac{y^{2-\beta} + (1-y)^{2-\beta}}{\Gamma(3-\beta)} - \frac{6(y^{3-\beta} + (1-y)^{3-\beta})}{\Gamma(4-\beta)} + \frac{12(y^{4-\beta} + (1-y)^{4-\beta})}{\Gamma(5-\beta)} \right\}.
 \end{aligned}$$

The analytical solution is $u(x, y, t) = (1+t^2)x^2(1-x)^2 y^2(1-y)^2$. To show the superiority of our methods as much as possible, we compare the spatial accuracy of the weighted and shifted GL (WSGL) methods [42] ($(p, q) = (1, 0)$ for WSGL1 and $(p, q) = (1, -1)$ for WSGL2, p, q are weighted parameters), FD method [7], FE method based on bilinear rectangular finite elements [37] and our DQ method based on Inverse Multiquadrics in terms of $\|u - U\|_{L^2}$. Here, we note that the structured quadrilateral meshes with the mesh sizes $h = 1/4$, $h = 1/8$, $h = 1/16$ and $h = 1/32$ are employed in the program running of the above FE method, i.e., the nodal numbers in turn are 25, 81, 289 and 1089, respectively. Taking $\theta = 0.5$, $\nu = 8$, $\sigma = q = 2$ and $\tau = 1.0 \times 10^{-3}$, the numerical errors at $t = 1$ of all the above-mentioned methods are reported in Table 5. From this table, we observe that the proposed DQ method is more accurate than WSGL and FD methods by using the same nodal numbers. Although the error magnitude of DQ method is about the same as bilinear rectangular FE method, it is certain that our method would be more flexible in implementation and have a less amount of computation than bilinear rectangular FE method because DQ methods do not require meshes generation in practical computation, nor is variational principle.

Furthermore, to get more insight into the computational efficiency of the proposed DQ method, we compare the spatial accuracy and CPU times of FE method based on linear unstructured triangular finite elements [49] and our DQ method with the same nodal numbers. Retaking $\theta = 1$, the numerical errors at $t = 1$ and the CPU time costs are all tabulated in Table 6, where the unstructured triangular meshes of the mesh sizes $h \approx 1/2$, $h \approx 1/4$, $h \approx 1/8$ and $h \approx 1/12$ are used in FE method with the nodal numbers exactly being 12, 37, 121 and 199, respectively. In Fig. 2, the used triangular meshes with $h \approx 1/8$ and $h \approx 1/12$ are displayed. The configuration of 199 nodes used in IMQ-based DQ method and its corresponding absolute error distribution of IMQ-based DQ method at $t = 1$ are presented in Fig. 3. From these table and figures, we observe that DQ method obtains more accurate numerical solutions than FE method, and not only that, the CPU times of our DQ method are far less than those of FE method, which further indicates

that our method causes the computational costs so much less than FE method. On the other hand, the absolute error reaches a maximum in the center of the square domain and gradually decreases along the center towards the boundary, which is related to the shape of the analytical solution.

Table 5: The comparison of mean-square errors at $t = 1$ for WSGL, FD, FE and DQ methods when $q = 2$, $\theta = 0.5$ and $\alpha = \beta = 1.6$

M	WSGL1 [42]	WSGL2 [42]	FD method [7]	FE method [37]	IMQ-based DQ method
24	8.2885e-04	7.1069e-04	5.1926e-04	2.8397e-04	2.4378e-04
80	2.0070e-04	2.4232e-04	1.1762e-05	8.6729e-05	7.7419e-05
288	4.8865e-05	6.9518e-05	2.6904e-05	2.2360e-05	2.1523e-05
1088	1.1904e-05	1.8377e-05	6.2224e-06	5.1208e-06	6.5475e-06

Table 6: The comparison of errors at $t = 1$ and CPU times for FE and DQ methods when $q = 2$, $\theta = 1$ and $\alpha = \beta = 1.6$

M	FE method [49]			IMQ-based DQ method		
	$\ u - U\ _{L^2}$	$\ u - U\ _{L^\infty}$	CPU times/s	$\ u - U\ _{L^2}$	$\ u - U\ _{L^\infty}$	CPU times/s
11	1.4364e-03	1.9251e-03	8.4470	5.7675e-04	1.1361e-03	5.2219
36	3.8724e-04	4.1695e-04	34.0283	1.1968e-04	2.6712e-04	15.1634
120	1.2548e-04	1.9499e-04	138.7742	2.1899e-05	4.7802e-05	46.0256
198	7.8313e-05	1.2380e-04	240.2891	1.0404e-05	2.2870e-05	77.1730

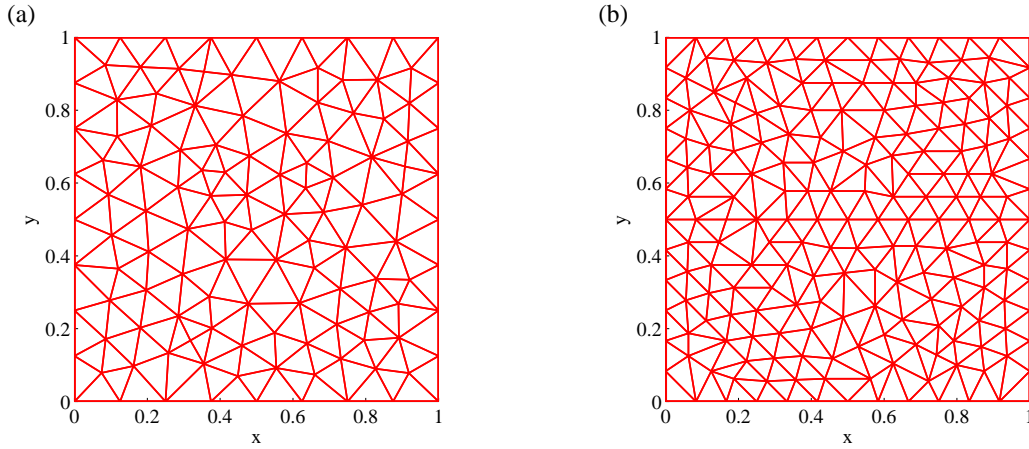


Figure 2: The unstructured triangular meshes used by FE method with the mesh sizes $h \approx 1/8$ and $h \approx 1/12$, respectively.

Example 6.4. Consider the two-dimensional multi-term TSFPDE:

$$\begin{cases} \sum_{r=1}^3 a_{r0}^C D_t^{\theta_r} u(x, y, t) - \frac{x^\alpha}{2} \frac{\partial_+^\alpha u(x, y, t)}{\partial x_+^\alpha} - \frac{y^\beta}{2} \frac{\partial_+^\beta u(x, y, t)}{\partial y_+^\beta} = f(x, y, t), & (x, y, t) \in \Omega \times (0, T], \\ u(x, y, 0) = 0, & (x, y) \in \Omega, \\ u(x, y, t) = t^3 x^2 y^2, & (x, y, t) \in \partial\Omega \times (0, T], \end{cases} \quad (5.33)$$

on the triangular domain $\Omega = \{(x, y) | 0 \leq x \leq 1, 0 \leq y \leq 1 - x\}$ with $a_1 = 2$, $a_2 = 0.5$, $a_3 = 3$, $\theta_1 = 0.1$, $\theta_2 = 0.3$,

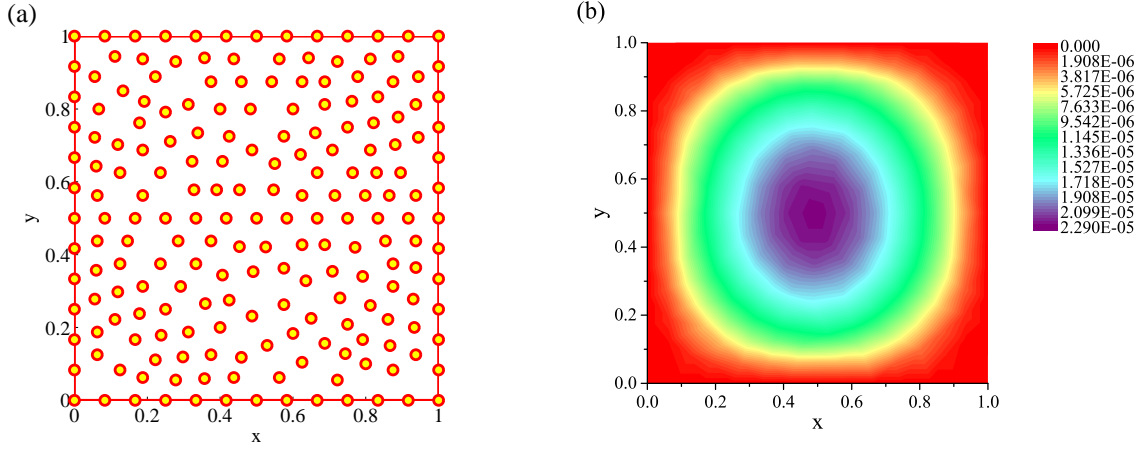


Figure 3: The configuration of 199 nodes and its absolute error distribution of IMQ-based DQ method at $t = 1$.

$\theta_3 = 0.5$, $\alpha = 1.5$, $\beta = 1.8$ and the source term

$$f(x, y, t) = \sum_{r=1}^3 \frac{6a_r t^{3-\theta_r} x^2 y^2}{\Gamma(4-\theta_r)} - t^3 x^2 y^2 \left\{ \frac{1}{\Gamma(3-\alpha)} + \frac{1}{\Gamma(3-\beta)} \right\}.$$

The analytical solution is $u(x, y, t) = t^3 x^2 y^2$. We use Multiquadrics and Gaussian as the trial functions and choose the corresponding free parameters by $\nu = 0.3$, $\sigma = 1$ and $\nu = 0.5$, $\sigma = 1$, respectively. The convergent results at $t = 0.5$ with $q = 3$ and $\tau = 1.0 \times 10^{-3}$ are reported in Table 7. In Fig. 4, we show the used configuration of 152 nodes and its corresponding absolute error distribution of GA-based DQ method at $t = 0.5$. It can be seen from the table and figure that the proposed DQ methods are convergent to the analytical solution as the nodal number increases. For this problem, the accuracy of MQ-based DQ method is higher than GA-based DQ method either in sense of mean-square error or maximum error, that is to say, MQ-based DQ method creates better numerical solution than GA-based DQ method. Moreover, the absolute error of GA-based DQ method is relatively large around the hypotenuse of this triangular domain and gradually decreases along the hypotenuse towards its two right-angle sides.

Table 7: The convergent results at $t = 0.5$ with $q = 3$, $\tau = 1.0 \times 10^{-3}$ and different M for Example 6.4

M	MQ-based DQ method		GA-based DQ method	
	$\ u - U\ _{L^2}$	$\ u - U\ _{L^\infty}$	$\ u - U\ _{L^2}$	$\ u - U\ _{L^\infty}$
55	5.7083e-05	1.8789e-04	8.2862e-05	3.0100e-04
79	4.4719e-05	1.6652e-04	5.9078e-05	2.2586e-04
114	3.8698e-05	1.5015e-04	5.2482e-05	2.0574e-04
152	2.9558e-05	1.1855e-04	3.6037e-05	1.5203e-04

Example 6.5. Consider the two-dimensional multi-term TSFPDE:

$$\begin{cases} \sum_{r=1}^3 a_{r0}^C D_t^{\theta_r} u(x, y, t) + \frac{1}{2 \cos(\alpha\pi/2)} \left(\frac{\partial_+^\alpha u(x, y, t)}{\partial x_+^\alpha} + \frac{\partial_-^\alpha u(x, y, t)}{\partial x_-^\alpha} \right) \\ + \frac{1}{2 \cos(\beta\pi/2)} \left(\frac{\partial_+^\beta u(x, y, t)}{\partial y_+^\beta} + \frac{\partial_-^\beta u(x, y, t)}{\partial y_-^\beta} \right) = f(x, y, t), & (x, y, t) \in \Omega \times (0, T], \\ u(x, y, 0) = (4x^2 + y^2 - 1)^2/10, & (x, y) \in \Omega, \\ u(x, y, t) = 0, & (x, y, t) \in \partial\Omega \times (0, T], \end{cases} \quad (5.34)$$

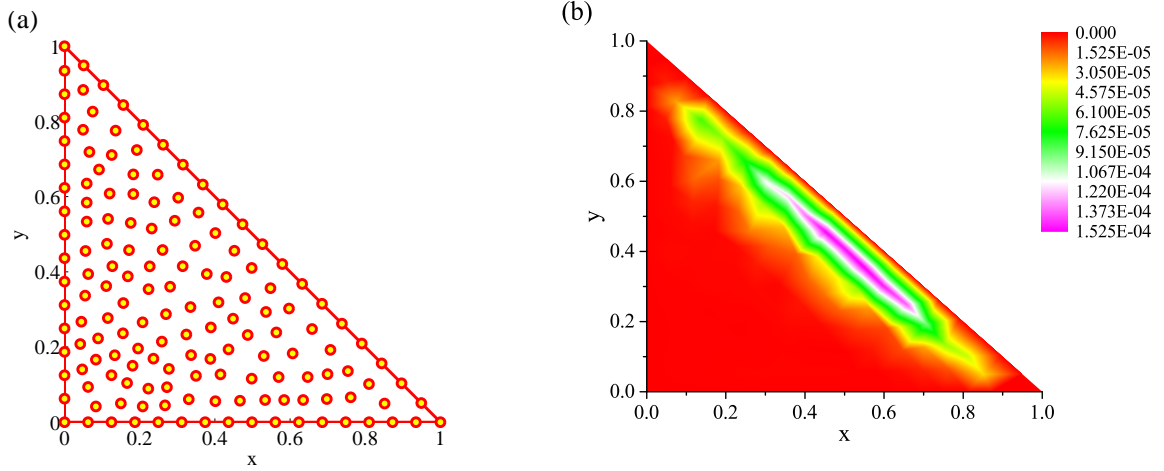


Figure 4: The configuration of 153 nodes and its absolute error distribution of GA-based DQ method at $t = 0.5$.

on the elliptical domain $\Omega = \{(x, y) | 4x^2 + y^2 \leq 1\}$ with $a_1 = a_2 = a_3 = 1$, $\theta_1 = 0.6$, $\theta_2 = 0.7$, $\theta_3 = 1$, $\alpha = \beta = 1.6$ and the source term

$$\begin{aligned}
 f(x, y, t) = & \sum_{r=1}^3 \frac{a_r t^{2-\theta_r}}{5\Gamma(3-\theta_r)} (4x^2 + y^2 - 1)^2 \\
 & + \frac{(1+t^2)}{20 \cos(\alpha\pi/2)} \left\{ (192x_l^2 + 16y^2 - 16) \frac{(x-x_l)^{2-\alpha}}{\Gamma(3-\alpha)} + \frac{384x_l(x-x_l)^{3-\alpha}}{\Gamma(4-\alpha)} + \frac{384(x-x_l)^{4-\alpha}}{\Gamma(5-\alpha)} \right. \\
 & + (192x_r^2 + 16y^2 - 16) \frac{(x_r-x)^{2-\alpha}}{\Gamma(3-\alpha)} + \frac{384x_r(x_r-x)^{3-\alpha}}{\Gamma(4-\alpha)} + \left. \frac{384(x_r-x)^{4-\alpha}}{\Gamma(5-\alpha)} \right\} \\
 & + \frac{(1+t^2)}{20 \cos(\beta\pi/2)} \left\{ (192y_l^2 + 16x^2 - 16) \frac{(y-y_l)^{2-\beta}}{\Gamma(3-\beta)} + \frac{384y_l(y-y_l)^{3-\beta}}{\Gamma(4-\beta)} + \frac{384(y-y_l)^{4-\beta}}{\Gamma(5-\beta)} \right. \\
 & + (192y_r^2 + 16x^2 - 16) \frac{(y_r-y)^{2-\beta}}{\Gamma(3-\beta)} + \frac{384y_r(y_r-y)^{3-\beta}}{\Gamma(4-\beta)} + \left. \frac{384(y_r-y)^{4-\beta}}{\Gamma(5-\beta)} \right\},
 \end{aligned}$$

with $x_l = -\sqrt{1-y^2}/2$, $x_r = \sqrt{1-y^2}/2$, $y_l = -\sqrt{1-4x^2}$ and $y_r = \sqrt{1-4x^2}$.

The analytical solution is $u(x, y, t) = \frac{1+t^2}{10} (4x^2 + y^2 - 1)^2$. We compare the spatial accuracy of FE method [28] and our DQ methods based on Inverse Quadratics and Gaussians in terms of $\|u - U\|_{L^2}$, where we choose the free parameters by $\nu = 11$, $\sigma = 2$ for Inverse Quadratics while $\nu = 4.5$, $\sigma = 2$ for Gaussians. Taking $q = 2$ and $\tau = 1.0 \times 10^{-3}$, the numerical errors at $t = 1$ of FE and DQ methods are all tabulated in Table 8. The used configurations of 113, 239 and 413 nodes and their corresponding absolute error distributions of IQ-based DQ method at $t = 1$ are displayed in Fig. 5. In the computation, N_e is the total number of triangles of the meshes used by the FE method. In Table 8, it can be seen that N_e is taken to be 70, 468, 1142 and 1738, respectively, then according to the proportional relationship between the numbers of nodes and triangles in a triangular mesh (the proportion of numbers of nodes to triangles is about 3:1), we know that the nodal number is bound to be much larger than N_e . Thus, we conclude that our DQ methods produce the same error magnitude as FE method with much less nodal numbers, which further confirms the effectiveness and advantages of our methods. Besides, the absolute error reaches a maximum in the center of this elliptical domain and gradually decreases along the center towards its boundary, this is because the change of analytical solution is relatively rapid around the center of this domain and becomes gentle in other places.

Table 8: The comparison of mean-square errors at $t = 1$ for FE and DQ methods when $\theta_1 = 0.6$, $\theta_2 = 0.7$, $\theta_3 = 1$ and $\alpha = \beta = 1.6$.

N_e	FE method [28]	M	IQ-based DQ method		GA-based DQ method	
	$\ u - U\ _{L^2}$		$\ u - U\ _{L^2}$	$\ u - U\ _{L^\infty}$	$\ u - U\ _{L^2}$	$\ u - U\ _{L^\infty}$
70	8.6311e-03	34	7.4516e-03	1.5952e-02	6.7396e-03	1.4335e-02
468	1.4508e-03	112	1.2389e-03	3.1296e-03	1.3671e-03	3.5605e-03
1142	5.4919e-04	238	6.6484e-04	1.4906e-03	7.3477e-04	1.7147e-03
1738	3.6969e-04	412	4.2034e-04	9.4854e-04	4.1947e-04	1.0285e-03

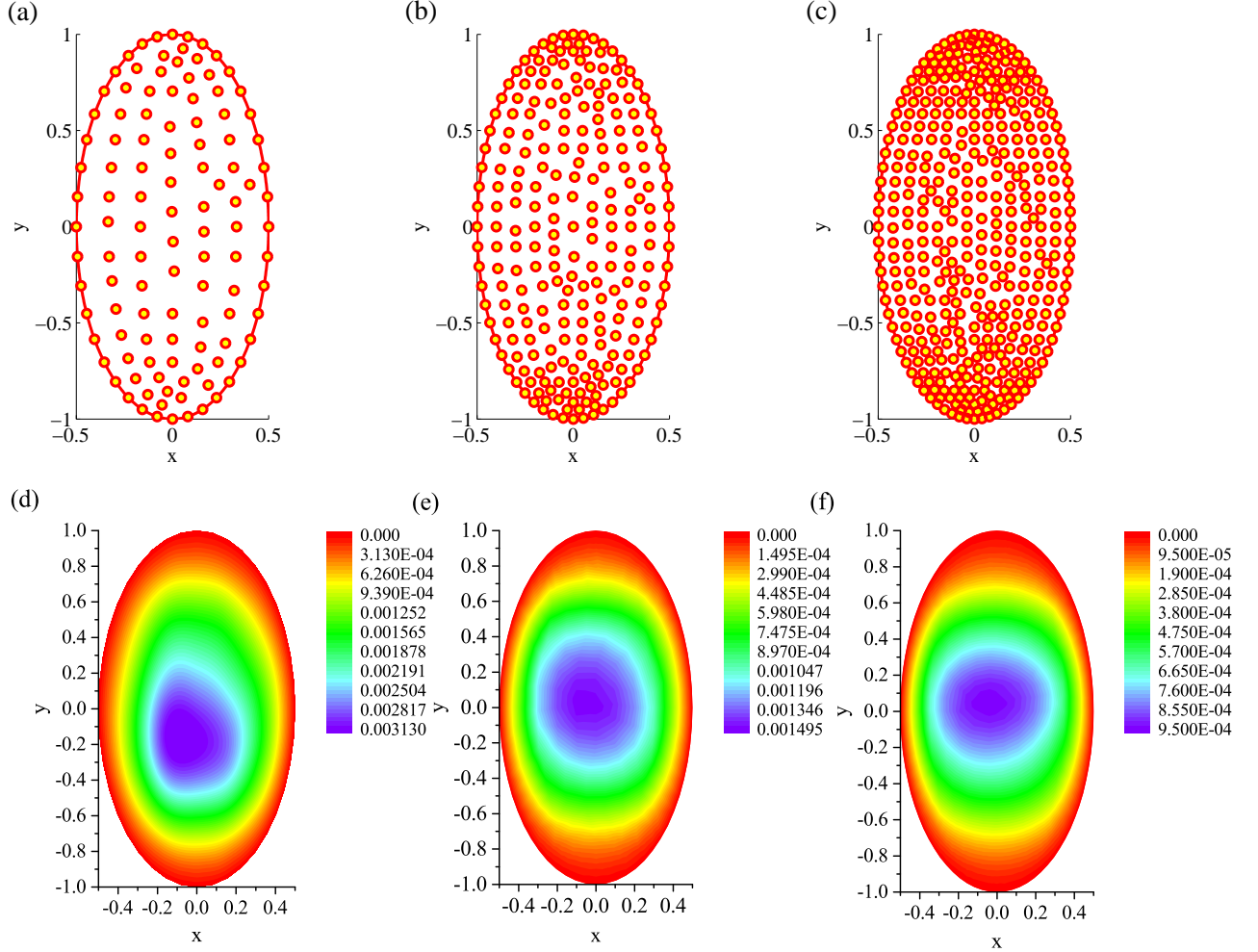


Figure 5: The configurations of 113, 239 and 413 nodes and their absolute error distributions of IQ-based DQ method at $t = 1$.

5.3. Three-dimensional problems

Example 6.6. Consider the three-dimensional multi-term TSFDE:

$$\begin{cases} \sum_{r=1}^4 a_r D_t^{\theta_r} u(x, y, z, t) - \frac{y^\gamma}{2} \frac{\partial^\gamma u(x, y, z, t)}{\partial z_-^\gamma} = f(x, y, z, t), & (x, y, z; t) \in \Omega \times (0, T], \\ u(x, y, z, 0) = 0, & (x, y, z) \in \Omega, \\ u(x, y, z, t) = t^3 y^{2-\gamma} (1-x-y-z)^2, & (x, y, z; t) \in \partial\Omega \times (0, T], \end{cases} \quad (5.35)$$

on the triangular pyramid domain $\Omega = \{(x, y, z) | 0 \leq x, y \leq 1, 0 \leq z \leq 1-x-y\}$ with $\theta_1 = 2, \theta_2 = 1.5, \theta_3 = 2, \theta_4 = 1, a_1 = 0.2, a_2 = 0.4, a_3 = 0.7, a_4 = 0.9, \gamma = 1.8$ and the source term

$$f(x, y, z, t) = \sum_{r=1}^4 \frac{6a_r t^{3-\theta_r}}{\Gamma(4-\theta_r)} y^{2-\gamma} (1-x-y-z)^2 - \frac{t^3 y^2 (1-x-y-z)^{2-\gamma}}{\Gamma(3-\gamma)},$$

The analytical solution is given by $u(x, y, z, t) = t^3 y^{2-\gamma} (1-x-y-z)^2$. We test the convergent behavior in space by using Inverse Multiquadrics and Inverse Quadratics as the trial functions with the nodal numbers being 91, 119, 165 and 214. The corresponding shape parameters are selected by 0.1, 0.2, 0.9, 1 for Inverse Multiquadrics and 0.08, 0.16, 0.7, 0.8 for the latter. The convergent results at $t = 0.5$ with $q = 2$ and $\tau = 5.0 \times 10^{-4}$ are listed in Table 9. The used configuration of 119 nodes and its corresponding absolute error distribution of IMQ-based DQ method at $t = 0.5$ are displayed in Fig. 6, respectively. It is observed from this table and figure that the errors of these two DQ methods are convergent to the analytical solution with a high enough accuracy, which implies that our DQ methods are effective for the three-dimensional multi-term TSFPDEs. The absolute error of IMQ-based DQ method is relatively large at the nodes near the center of this triangular pyramid domain and the further the node from its center, the smaller the error looks like, which coincides with the change of analytical solution. Moreover, IMQ-based DQ method produces nearly the same accuracy as IQ-based DQ method by using the above parameters.

Table 9: The convergent results at $t = 0.5$ with $q = 2$ and $\tau = 5.0 \times 10^{-4}$ for Example 6.6

M	IMQ-based DQ method		IQ-based DQ method	
	$\ u - U\ _{L^2}$	$\ u - U\ _{L^\infty}$	$\ u - U\ _{L^2}$	$\ u - U\ _{L^\infty}$
90	1.1210e-04	7.5967e-04	1.0397e-04	6.2086e-04
118	5.9533e-05	4.3038e-04	7.8823e-05	5.0199e-04
164	4.6240e-05	3.2299e-04	4.7980e-05	3.3329e-04
213	4.1000e-05	2.4174e-04	4.2061e-05	2.6229e-04

Example 6.7. Consider the three-dimensional multi-term TSFDE:

$$\begin{cases} \frac{{}_0^C D_t^{\theta_1} u(x, y, z, t) + 3{}_0^C D_t^{\theta_2} u(x, y, z, t)}{2} - \frac{(y - 0.5 + \sqrt{0.25 - (x - 0.5)^2 - z^2})^\beta}{6} \frac{\partial^\beta u(x, y, z, t)}{\partial y_+^\beta} \\ = f(x, y, z, t), & (x, y, z; t) \in \Omega \times (0, T], \\ u(x, y, z, 0) = 0, & (x, y, z) \in \Omega, \\ u(x, y, z, t) = (1 + t^4)(y - 0.5 + \sqrt{0.25 - (x - 0.5)^2 - z^2})^3 z^3, & (x, y, z; t) \in \partial\Omega \times (0, T], \end{cases} \quad (5.36)$$

on the sphere domain $\Omega = \{(x, y, z) | (x - 0.5)^2 + (y - 0.5)^2 + z^2 \leq 0.25\}$ with $\theta_1 = 0.3, \theta_2 = 0.8$ and $\beta = 1.9$. The source term is given as follows

$$f(x, y, z, t) = \left\{ \frac{12t^{4-\theta_1}}{\Gamma(5-\theta_1)} + \frac{36t^{4-\theta_2}}{\Gamma(5-\theta_2)} \right\} (y - 0.5 + \sqrt{0.25 - (x - 0.5)^2 - z^2})^3 z^3 - \frac{(1 + t^4)(y - 0.5 + \sqrt{0.25 - (x - 0.5)^2 - z^2})^3 z^3}{\Gamma(4-\beta)},$$

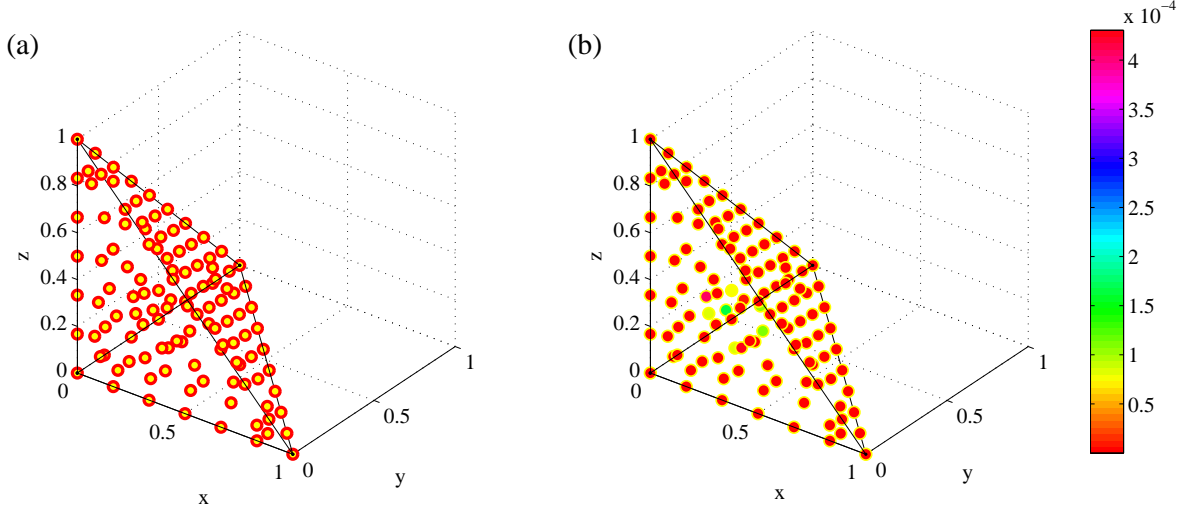


Figure 6: The configuration of 119 nodes and its absolute error distribution of IMQ-based DQ method at $t = 0.5$.

to enforce the analytical solution $u(x, y, z, t) = (1 + t^4)(y - 0.5 + \sqrt{0.25 - (x - 0.5)^2 - z^2})^3 z^3$.

In this test, we select $q = 4$, $\tau = 1.0 \times 10^{-3}$ and report the convergent results at $t = 0.5$ in Table 10, where Multiquadrics and Inverse Multiquadrics are used as the trial functions and the free parameters are chosen to be $\nu = 3$, $\sigma = 1$ and $\nu = 3.3$, $\sigma = 1$, respectively. Also, we highlight the used configuration of 181 nodes and its corresponding absolute error distribution of MQ-based DQ method at $t = 0.5$ in Fig. 7. The results observed from the table and figure illustrate that the proposed DQ methods create the numerical solutions which are in excellent agreement with the analytical solution and the errors produced by these two DQ methods do not differ significantly under the selected parameters. Besides, The absolute error distribution of MQ-based DQ method coincides with the change of analytical solution. Therefore, our DQ methods are effective for the three-dimensional multi-term TSFPDEs.

Table 10: The convergent results at $t = 0.5$ with $q = 4$ and $\tau = 1.0 \times 10^{-3}$ for Example 6.7

M	MQ-based DQ method		IMQ-based DQ method	
	$\ u - U\ _{L^2}$	$\ u - U\ _{L^\infty}$	$\ u - U\ _{L^2}$	$\ u - U\ _{L^\infty}$
73	1.7998e-04	8.8476e-04	1.6390e-04	8.4253e-04
101	1.2964e-04	8.0668e-04	1.2897e-04	8.1281e-04
180	5.7266e-05	4.6403e-04	5.9258e-05	4.7803e-04
336	2.1243e-05	1.3452e-04	2.2835e-05	1.4298e-04

6. Conclusion

In this investigation, an advanced DQ technique was developed to obtain the numerical solutions of the multi-term TSFPDEs on two- and three-dimensional general domains. The considered problem was reduced into a group of multi-term fractional ODEs by a new class of DQ formulas to approximate fractional derivatives with the help of some familiar RBFs as trial functions. A fully discrete RBFs-based DQ scheme has been derived by applying a family of high-order difference schemes to discretize the resulting multi-term fractional ODEs, which possesses the advantages of small computational cost, easy programming, and vast flexibility in implementation as the traditional DQ methods. In numerical tests, we used the proposed DQ method to tackle the problems on square, triangular, elliptical, triangular pyramid and sphere domains. It produces very satisfactory accuracy both in time and space, and the numerical results and comparisons with the true solutions or the errors yielded by the other methods like FE method illustrate that our

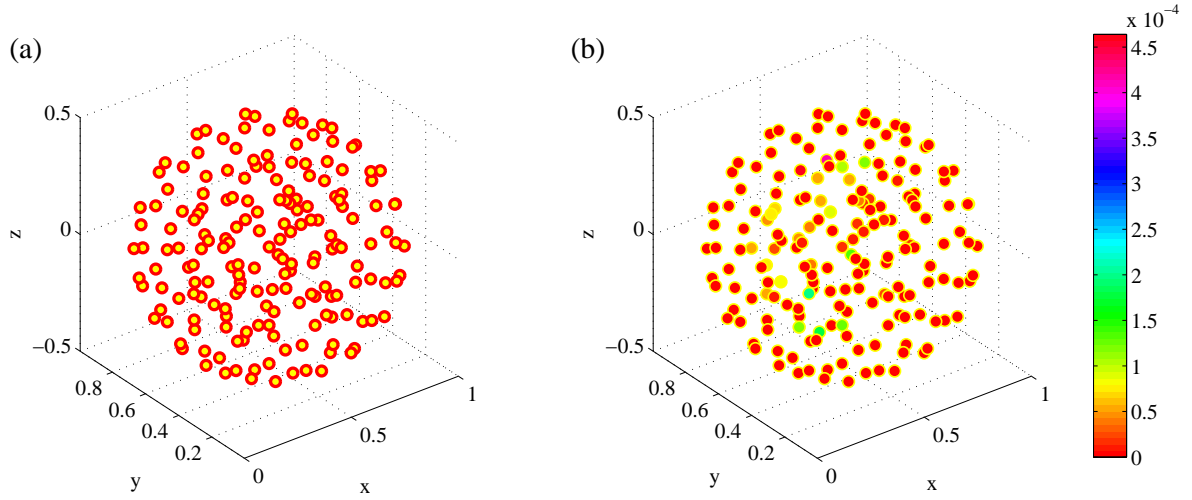


Figure 7: The configuration of 181 nodes and its absolute error distribution of MQ-based DQ method at $t = 0.5$.

method is effective or even more favorable on the aspect of computational accuracy.

Acknowledgement: This research was supported by the Natural Science Foundation of Hunan Province of China (Nos. 2020JJ506, 2020JJ1476), the Scientific Research Funds of Hunan Provincial Education Department (Nos. 19B509, 19C1643) and the National Natural Science Foundation of China (No. 11971386).

References

- [1] E.E. Adams, L.W. Gelhar, Field study of dispersion in a heterogeneous aquifer: 2. spatial moments analysis, *Water Res. Research* 28(12) (1992) 3293–3307.
- [2] S.N. Atluri, T.L. Zhu, A new meshless local Petrov-Galerkin (MLPG) approach in computational mechanics, *Comput. Mech.* 22 (1998) 117–127.
- [3] R. Bellman, B. Kashef, E.S. Lee, R. Vasudevan, Differential quadrature and splines, *Comput. Math. Appl.* 1 (1975) 371–376.
- [4] T. Belytschko, Y.Y. Lu, L. Gu, Element-free Galerkin methods, *Int. J. Numer. Meth. Eng.* 37 (1994) 229–256.
- [5] A.H. Bhrawy, D. Baleanu, A spectral Legendre-Gauss-Lobatto collocation method for a space-fractional advection diffusion equations with variable coefficients, *Rep. Math. Phys.* 72 (2013) 219–233.
- [6] A.H. Bhrawy, M.A. Zaky, A method based on the Jacobi tau approximation for solving multi-term time-space fractional partial differential equations, *J. Comput. Phys.* 281 (2015) 876–895.
- [7] C. Çelik, M. Duman, Crank-Nicolson method for the fractional diffusion equation with the Riesz fractional derivative, *J. Comput. Phys.* 231 (2012) 1743–1750.
- [8] M.H. Chen, W.H. Deng, Fourth order difference approximations for space Riemann-Liouville derivatives based on weighted and shifted Lubich difference operators, *Commun. Comput. Phys.* 16 (2014) 516–540.
- [9] A.H.D. Cheng, Multiquadric and its shape parameter-A numerical investigation of error estimate, condition number, and round-off error by arbitrary precision computation, *Eng. Anal. Bound. Elem.* 36 (2012) 220–239.
- [10] J.Q. Cheng, B. Wang, S.Y. Du, A theoretical analysis of piezoelectric/composite laminate with larger-amplitude deflection effect, Part II: Hermite differential quadrature method and application, *Int. J. Solids. Struct.* 42 (2005) 6181–6201.
- [11] R.J. Cheng, F.X. Sun, J.F. Wang, Meshless analysis of two-dimensional two-sided space-fractional wave equation based on improved moving least-squares approximation, *Int. J. Comput. Math.* 95 (2018) 540–560.
- [12] M. Dehghan, M. Abbaszadeh, An efficient technique based on finite difference/finite element method for solution of two-dimensional space/multi-time fractional Bloch-Torrey equations, *Appl. Numer. Math.* 131 (2018) 190–206.
- [13] W.H. Deng, Finite element method for the space and time fractional Fokker-Planck equation, *SIAM J. Numer. Anal.* 47 (2008) 204–226.
- [14] H. Du, M.K. Lim, R.M. Lin, Application of generalized differential quadrature method to structural problems, *Int. J. Numer. Meth. Eng.* 37 (1994) 1881–1896.
- [15] V.J. Ervin, J.P. Roop, Variational formulation for the stationary fractional advection dispersion equation, *Numer. Meth. Part. D. E.* 22 (2006) 558–576.
- [16] W.P. Fan, X.Y. Jiang, F.W. Liu, V. Anh, The unstructured mesh finite element method for the two-dimensional multi-term time-space fractional diffusion-wave equation on an irregular convex domain, *J. Sci. Comput.* 77 (2018) 27–52.

- [17] A.I. Fedoseyev, M.J. Friedman, E.J. Kansa, Improved multiquadric method for elliptic partial differential equations via PDE collocation on the boundary, *Comput. Math. Appl.* 43 (2002) 439–455.
- [18] H.F. Fu, Y.N. Sun, H. Wang, X.C. Zheng, Stability and convergence of a Crank-Nicolson finite volume method for space fractional diffusion equations, *Appl. Numer. Math.* 139 (2019) 38–51.
- [19] W.M. Han, X.P. Meng, Error analysis of the reproducing kernel particle method, *Comput. Method. Appl. M.* 190 (2001) 6157–6181.
- [20] S.M. Hosseini, R. Ghaffari, Polynomial and nonpolynomial spline methods for fractional sub-diffusion equations, *Appl. Math. Model.* 38 (2014) 3554–3566.
- [21] C.B. Huang, X.J. Yu, C. Wang, Z.Z. Li, N. An, A numerical method based on fully discrete direct discontinuous Galerkin method for the time fractional diffusion equation, *Appl. Math. Comput.* 264 (2015) 483–492.
- [22] J.H. Jia, H. Wang, Fast finite difference methods for space-fractional diffusion equations with fractional derivative boundary conditions, *J. Comput. Phys.* 293 (2015) 359–369.
- [23] Y.J. Jiang, J.T. Ma, High-order finite element methods for time-fractional partial differential equations, *J. Comput. Appl. Math.* 235 (2011) 3285–3290.
- [24] E.J. Kansa, Multiquadrics-A scattered data approximation scheme with applications to computational fluid-dynamics-II solutions to parabolic, hyperbolic and elliptic partial differential equations, *Comput. Math. Appl.* 19 (1990) 147–161.
- [25] A.A.A. Kilbas, H.M. Srivastava, J.J. Trujillo, *Theory and Applications of Fractional Differential Equations*, Elsevier B. V., Amsterdam, 2006.
- [26] Y.M. Lin, C.J. Xu, Finite difference/spectral approximations for the time-fractional diffusion equation, *J. Comput. Phys.* 225 (2007) 1533–1552.
- [27] Z. Lin, F.W. Liu, D.D. Wang, Y.T. Gu, Reproducing kernel particle method for two-dimensional time-space fractional diffusion equations in irregular domains, *Eng. Anal. Bound. Elem.* 97 (2018) 131–143.
- [28] F.W. Liu, L.B. Feng, V. Anh, J. Li, Unstructured-mesh Galerkin finite element method for the two-dimensional multi-term time-space fractional Bloch-Torrey equations on irregular convex domains, *Comput. Math. Appl.* 78 (2019) 1637–1650.
- [29] F.W. Liu, P.H. Zhuang, I. Turner, V. Anh, K. Burrage, A semi-alternating direction method for a 2-D fractional FitzHugh-Nagumo monodomain model on an approximate irregular domain, *J. Comput. Phys.* 293 (2015) 252–263.
- [30] G.R. Liu, Y.T. Gu, A point interpolation method for two-dimensional solids, *Int. J. Numer. Meth. Eng.* 50 (2001) 937–951.
- [31] Q. Liu, F.W. Liu, Y.T. Gu, P.H. Zhuang, J. Chen, I. Turner, A meshless method based on Point Interpolation Method (PIM) for the space fractional diffusion equation, *Appl. Math. Comput.* 256 (2015) 930–938.
- [32] M.M. Meerschaert, C. Tadjeran, Finite difference approximations for fractional advection-dispersion flow equations, *J. Comput. Appl. Math.* 172(1) (2004) 65–77.
- [33] D.A. Murio, Implicit finite difference approximation for time fractional diffusion equations, *Comput. Math. Appl.* 56 (2008) 1138–1145.
- [34] B. Nayroles, G. Touzot, P. Villon, Generalizing the finite element method: diffuse approximation and diffuse elements, *Comput. Mech.* 10 (1992) 307–318.
- [35] G.F. Pang, W. Chen, K.Y. Sze, Gauss-Jacobi-type quadrature rules for fractional directional integrals, *Comput. Math. Appl.* 66 (2013) 597–607.
- [36] G.F. Pang, W. Chen, K.Y. Sze, Differential quadrature and cubature methods for steady-state space-fractional advection-diffusion equations, *Comput. Model. Eng. Sci.* 97 (2014) 299–322.
- [37] S.L. Qin, F.W. Liu, I. Turner, A 2D multi-term time and space fractional Bloch-Torrey model based on bilinear rectangular finite elements, *Commun. Nonlinear Sci.* 56 (2018) 270–286.
- [38] L.L. Qiu, W.H. Deng, J.S. Hesthaven, Nodal discontinuous Galerkin methods for fractional diffusion equations on 2D domain with triangular meshes, *J. Comput. Phys.* 298 (2015) 678–694.
- [39] J.R. Quan, C.T. Chang, New insights in solving distributed system equations by the quadrature method-I. Analysis, *Comput. Chem. Eng.* 13 (1989) 779–788.
- [40] J.C. Ren, Z.Z. Sun, X. Zhao, Compact difference scheme for the fractional sub-diffusion equation with Neumann boundary conditions, *J. Comput. Phys.* 232 (2013) 456–467.
- [41] A. Simmons, Q.Q. Yang, T. Moroney, A finite volume method for two-sided fractional diffusion equations on non-uniform meshes, *J. Comput. Phys.* 335 (2017) 747–759.
- [42] W.Y. Tian, H. Zhou, W.H. Deng, A class of second order difference approximations for solving space fractional diffusion equations, *Math. Comput.* 84 (2015) 1703–1727.
- [43] Y.L. Wu, C. Shu, Development of RBF-DQ method for derivative approximation and its application to simulate natural convection in concentric annuli, *Comput. Mech.* 29 (2002) 477–485.
- [44] Z.Z. Yang, Z.B. Yuan, Y.F. Nie, J.G. Wang, X.G. Zhu, F.W. Liu, Finite element method for nonlinear Riesz space fractional diffusion equations on irregular domains, *J. Comput. Phys.* 330 (2017) 863–883.
- [45] S.B. Yuste, Weighted average finite difference methods for fractional diffusion equations, *J. Comput. Phys.* 216 (2006) 264–274.
- [46] F.H. Zeng, F.W. Liu, C.P. Li, K. Burrage, I. Turner, V. Anh, A Crank-Nicolson ADI spectral method for a two-dimensional Riesz space fractional nonlinear reaction-diffusion equation, *SIAM J. Numer. Anal.* 52 (2014) 2599–2622.
- [47] H. Zhang, F.W. Liu, V. Anh, Galerkin finite element approximations of symmetric space fractional partial differential equations, *Appl. Math. Comput.* 217 (2010) 2534–2545.
- [48] J.Y. Zhang, G.W. Yan, Lattice Boltzmann method for the fractional sub-diffusion equation, *Int. J. Numer. Meth. Fl.* 80 (2016) 490–507.
- [49] X.G. Zhu, Y.F. Nie, J.G. Wang, Z.B. Yuan, A numerical approach for the Riesz space-fractional Fisher equation in two-dimensions, *Int. J. Comput. Math.* 94 (2017) 296–315.